Waveforms MOdels for Machine Type CommuNication inteGrating 5G Networks (WONG5) Document Number D3.2 New methods to enhance the energy efficiency

Yves Louët, Hmaied Shaiek, Daniel Roviras, Yahia Medjahdi, Rafik Zayani, Mouna Ben Mabrouk

Waveforms MOdels for Machine Type CommuNication inteGrating 5G Networks

(WONG5)

Document Number D3.2

New methods to enhance the energy efficiency

Contractual date of delivery:	12/10/2017
Project Number and Acronym:	ANR-15-CE25-0005, WONG5
Editor:	CentraleSupélec
Authors:	Yves LOUET, Hmaied SHAIEK, Daniel ROVIRAS, Yahia MEDJAHDI, Rafik ZAYANI, Mona BEN MABROUK
Participants:	CS, CNAM
Workpackage:	WP3
Security:	PR
Nature:	Report
Version:	0.1
Total Number of Pages:	57

Abstract:

This deliverable presents several signal processing methods to increase the efficiency of power amplifiers used in the MTC context. The considered waveforms are WOLA-OFDM, UFMC, f-OFDM and BF-OFDM and the PAPR reduction methods used are Tone Reservation, Selected Mapping and pre-coding. To take into account the power amplifier non linearity the deliverable proposes a joint approach combining a PAPR reduction method with a linearization technique.

Keywords: Power amplifier models, IBO, PAPR, OOB, PAPR reduction techniques, PA linearization, DPD.

Executive Summary

This document gathers peak to average power ratio (PAPR) reduction methods applied to post-OFDM waveforms in order to increase the efficiency of the power amplifier. The considered post-OFDM waveforms have been studied in previous works of WONG5 project and their performance stated in deliverable 2.2 and espacially in deliverable 3.1. In the 3.1 document, it has been shown that in presence of a nonlinear HPA, the performance of all the studied waveforms are affected in terms of power spectral density and symbol error rate. This leads to consider signal processing methods to mitigate the PAPR and to increase the power amplifier linearity. This is the objective of this deliverable (3.2) whose outline is as follows :

- section 2 : recall of selected waveforms and power amplifier model
- section 3 : PAPR reduction techniques (state of the art and proposed methods)
- section 4 : a proposed joint PAPR and linearization technique

Table of Contents

1. Introduction

Currently, one of the biggest challenge in telecommunications is to reduce the energy consumption of Base Stations (BSs) which consums about 80% of the total energy of cellular infrastructure. In fact, in today's macro base stations, the high Power Amplifier (PA) efficiency plays a key role in the energy efficiency of the whole transmitter chain as the PA is one of the most power-consuming components. For example, the PA accounts for 55-60% [Hil13] of the overall power consumption at full load in a LTE macro base station.

There are three levels to increase the efficiency of the power amplifier :

- The first level regards the transmitter device itself. In this way the idea is to modify the transmitter architecture. Several solutions have been proposed like envelope tracking, Doherty amplifiers, Kahn techniques, parallel architectures, LINC architectures and so one. The drawbacks of these techniques may lie in the increase of the architecture complexity.
- The second level is the signal processing level. Without any change in the amplifier architecture, the efficiency is increased with the help of peak to average power ratio reduction techniques, digital predistorsion techniques and in a few word thanks to all techniques which intend to mitigate the power amplifier input back-off.
- The third level regards the network level. In this context, the power efficiency is increased while using smaller cells so that the transmitted power is decreased compared to larger cells. Adding to this, the idea to reduce the power amplifier activation could be a good solution as well (on/off techniques). In this way the operating point of the power amplifier can be updated according to the load of the cell (night and day traffic changes). This issue is highly related to the first item (ie an update of the power amplifier architecture).

As a result, increasing the power amplifier efficiency could be a mixed of all the aforementionned techniques. For example some works combine envelope tracking, PAPR reduction and on/off techniques [Bra12].

In this document, we focused our work on the signal processing level with PAPR reduction techniques. The signal to be amplified is a multi-carrier signal (generated with post-OFDM modulations) whose PAPR levels are similar to those observed with regular OFDM signal. As said PAPR reduction techniques aim to decrease the input back-off. There are many PAPR reduction techniques whose performance could be very different depending on several criteria : their complexity, the receiver modification (known as downward compatibility), the bit error rate degradation, the out-of band regrowth, etc.

In this document we focused on powerfull PAPR reduction techniques (Tone Reservation, Selected Mapping, pre-coding) to be applied to WOLA-OFDM, UFMC, F-OFDM and BF-OFDM.

2. Selected waveforms and PA models

2.1 Selected waveforms

As a reminder, at the end of deliverable D2.1, the selected set of candidate waveforms (WF) for C-MTC was as following:

- CP-OFDM (taken as basis of comparison)
- Waveforms with complex orthogonality and filtering applied to a group of subcarriers:
  - WOLA-OFDM
  - UFMC/UF-OFDM
  - f-OFDM
- Waveforms with real orthogonality and filtering applied to single subcarrier :
  - FBMC-OQAM

The results obtained by task 2.2 concerning the proposition of new WFs for C-MTC have put in light several new possibilities. Among them, two WFs are very attractive for C-MTC: BF-OFDM and FFT-FBMC. These two WFs have a very good frequency localization thanks to a filter bank structure at the emitter side. The frequency localized filter is applied to groups of subcarriers as for UFMC and f-OFDM. These two WFs have a good resistance towards asynchronous users. At the receiver side, BF-OFDM uses the classical CP-OFDM receiver while FFT-FBMC uses the same filter bank as the emitter side. Because of these different receiver filters, BF-OFBM is more sensitive to asynchronous users than FFT-FBMC. Furthermore, for the two WFs, the orthogonality is in the complex domain, permitting to adapt very easily all classical MIMO techniques. Concerning complexity, results presented in D2.2 show an increase by a factor of 2 for the emitter (related to CP-OFDM) . For BF-OFDM the receiver complexity is slightly lower than the one of CP-OFDM while it remains in the order of a factor 2 for FFT-FBMC. In the deliverable D3.2, we will adress the problem of PAPR reduction for the selected WFs. From this point of view, the two WFs, BF-OFDM and FFT-FBMC, are similar because they use a similar emitter architecture. Hence, for this deliverable, we have chosen to study only BF-OFDM. The obtained results will be totally transposable to FFT-FBMC.

Concerning FBMC-OQAM an extensive work has been done in the recent years concerning PAPR reduction techniques and PA linearization. PAPR reduction techniques using Selective mapping (SLM) [SSJ06], [BSR15a], [BSR16b], [BSRRZ17] and Tone reservation (TR) [LQH13], [BSR15b], [Bul16] have been adapted to this WF. Active constellation extension (ACE) [NMdL$^+$14], Clipping [KVH$^+$14] and Partial transmit sequence (PTS) [QLJ13] techniques have also been adapted to FBMC. Linearization using digital predistorsion has been studied for FBMC-OQAM [BSR16a]. Due to this recent and intensive research results, FBMC-OQAM will not be further studied in D3.2 concerning PAPR and linearization.

Finally, the waveforms that we will consider in deliverable D3.2 are the following:

- CP-OFDM (taken as basis of comparison),

- WOLA-OFDM
- UFMC/UF-OFDM
- f-OFDM
- BF-OFDM

2.2 HPA models

The High Power Amplifier (HPA) models that will be used in the following of this deliverable are those introduced in section 2.2 of the deliverable D3.1. Two models will be used for simulations: a polynomial model fitting a realistic 3GPP HPA and a Rapp model.

2.2.1 Polynomial model fitting the 3GPP HPA

The first HPA, referred as 3GPP is a memoryless polynomial model. It corresponds to a $4\ GHz$ realistic HPA fitted with a polynomial model as provided in [R4-16]. The AM/AM and AM/PM conversions characteristics of this HPA are given in figures 2-1 and 2-2 respectively.

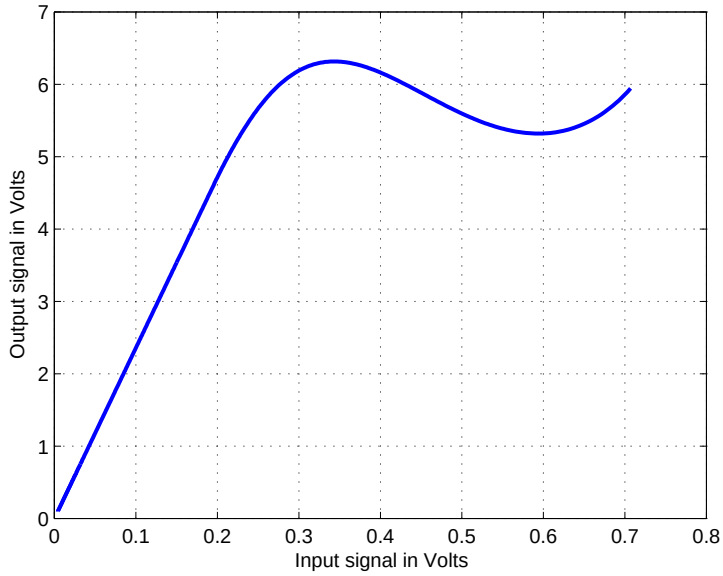

Figure 2-1: 3GPP HPA model: AM/AM conversion, input in volts, output in volts.

2.2.2 Rapp model

The signal at the HPA output can be written as follows:

$$u(t) = F_a(\rho(t))\exp(j\varphi(t)), \tag{2.1}$$

where $\rho(t)$ and $\varphi(t)$ are respectively the input signal ($x(t)$) modulus and phase. $F_a(\cdot)$ is the AM/AM conversion function, expressed, for the Rapp model, as follows:

$$F_a(\rho(t)) = \frac{G\rho(t)}{\left(1+\left|\frac{G\rho(t)}{A_{sat}}\right|^{2p}\right)^{\frac{1}{2p}}} \tag{2.2}$$

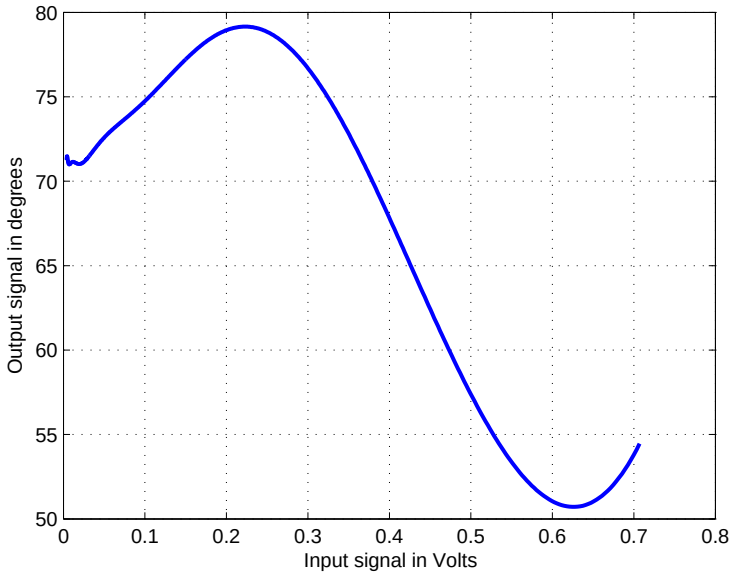

Figure 2-2: 3GPP HPA model: AM/PM conversion, input in volts, output in radian.

where G is the linear gain and A_{sat} is the saturation voltage. It's worth mentionning that Rapp model does not exhibit any phase distortion (i.e $F_p(\rho(t)) = 0$). The parameters G (slope of the curve of figure 2-1) and A_{sat} (saturation voltage) are chosen to be the same as the 3GPP HPA described in subsection 2.2.1. p is chosen to be 1.1 to have a different $-1dB$ compression point from the 3GPP HPA, as it can be seen in figure 2-3.

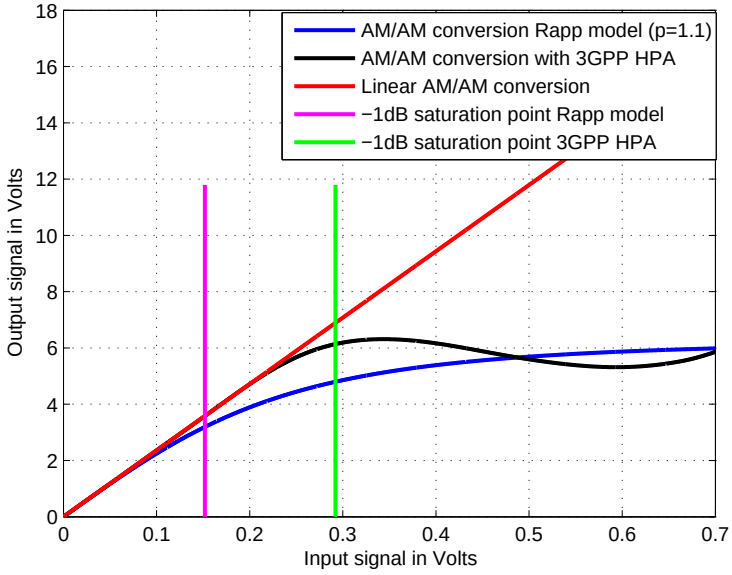

Figure 2-3: Rapp model: AM/AM-conversion comparison between the Rapp model and the 3GPP one, input in Volts, output in Volts.

3. PAPR reduction techniques

3.1 State of the art

As far as the PAPR problem is concerned, numerous PAPR reduction techniques have been proposed in literature for decades. As a result, many state of the art and surveys have been published on this issue as [LP08], [JY08], [Wun13]. In fact, PAPR reduction techniques can be classified in three top categories which are coding methods, probabilistic methods and adding signal methods. This section is dedicated to briefly introduce each of these categories and the criteria for PAPR reduction techniques selection.

3.1.1 Coding methods

When N signals are added with the same phase, they produce a peak power, which is N times the average power. Coding methods consist in reducing the occurrence probability of the same phase value of these signals. A simple block coding scheme was introduced in [AEJB94], and it consists in finding out all possible codewords and then select those codewords of lowest PAPR. It maps 3 bits data into 4 bits codeword by adding a Simple Odd Parity Code (SOBC) at the last bit across the channels. It has been shown that using this scheme the PAPR of the signal can be reduced from 6 dB to 2,5 dB. This technique has two limitations. First, an exhaustive search is required to find the best suitable codeword. Second, it also suffers from complexity to store large lookup tables for encoding and decoding in the transmitter and receiver respectively. In [Pop91], [TJZ04], authors used the Golay complementary sequences where more than 3 dB PAPR reduction has been obtained. In [DJ99], Davis et al. proposed codes with error correcting capabilities to achieve more lower PAPR for OFDM signals by determining the relationship of the cosets of Reed-Muller codes to Golay complementary sequences. However, for OFDM systems with large number of subcarriers, these block codes significantly reduce the transmission rate. In summary, the actual benefits of coding for PAPR reduction for practical multicarrier systems are limited, regarding the low coding rate, the intractable required search for a good code, as well as the prohibitively complexity for large number of subcarriers.

3.1.2 Probabilistic methods

The idea behind the probabilistic methods is to perform several copies of the initial signal by modifying the phase, amplitude and/or position of subcarriers and then select the copy with the minimum PAPR. These methods cannot guarantee the PAPR below a specified level. Moreover, it decreases the spectral efficiency, and the computational complexity increases as the number of subcarriers increases. The probabilistic methods include Selective Mapping (SLM) [BFH96], and Partial Transmit Sequence (PTS) [MH97] . A block diagram of SLM technique is shown in Figure 3-1.

In SLM, the input data sequences are multiplied by V different phase sequences to generate alternative input symbol sequences. Each of these alternative input data sequences are then applied to IFFT operation, and then the one with the lowest PAPR is selected for transmission. Therefore, its performance in reducing the PAPR directly depends on the number and the design of phase factors. The corresponding selected phase factor also needs to be transmitted to receiver as side information to properly

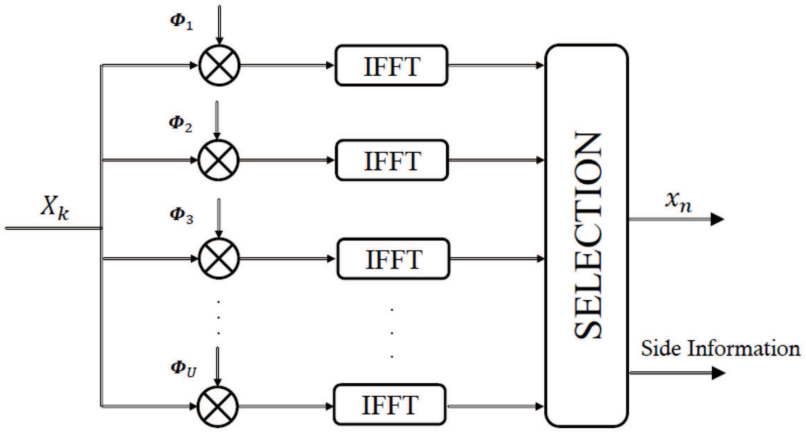

Figure 3-1: Illustration of SLM method.

extract the original information. Its major drawback is the high computational complexity and loss of bandwidth efficiency, since it needs U IFFT operations and ln U bits as side information. In addition, in case of loss of the side information during transmission, the whole data block is lost which signifficantly degrades the error performance of the system. Note that a novel SLM method has been proposed in [SYLGS99], for which no side information needs to be sent.

3.1.3 Adding methods

This category, as its name suggests, includes all techniques of PAPR reduction that can be formulated as PAPR(x + c_{papr}) < PAPR (x), where x refers to the OFDM signal and c_{papr} refers to the peak-reduction signal. Indeed, x and c_{papr} could be processed in time or frequency domain. In the literature, we find a large number of adding signal techniques such as clipping [LC97], Tone Reservation (TR) [Tel99], Tone Injection (TI) [Tel99], and Active Constellation Extension (ACE) [KJ03] to name a few.

3.1.3.1 Clipping

Clipping is one of the most used techniques for PAPR reduction due to its simplicity and its straightforward reduction gain. Its main objective is to constraint high amplitude peaks of a signal below a given threshold, without affecting its phase. Clipping falls under Adding Techniques category thanks to Bussgang theorem consequence : the output of any non linear system can be expressed as the sum of its input and an additional term. This technique results both in in-band and out-of-band distortions because of its nonlinear operation which degrades the system performance including Bit Error Rate (BER) and spectral efficiency. Filtering can reduce out of band radiation after clipping at the cost of peak re-growth so that, at some points, the signal after clipping and filtering will exceed the clipping threshold. Additionally, it changes the amplitude

probability distribution function of the signal and decreases the signal average power. To reduce the distortion effects of the clipping technique many other contributions were proposed in the literature to modify the clipping function such as deep clipping [SKO08], and the Invertible Clipping [SRL06].

3.1.3.2 Tone Reservation

The TR concept was introduced by Tellado in 1999 [Tel99]. This method is based on reserving subcarriers that do not carry any useful information and are called peak reduction tones. These tones are used for generating a PAPR reduction signal which when added to the original multicarrier signal decreases its peaks. The peak reduction tones and data tones are orthogonal to each other which makes recovering the data trivial. The principal of this technique is illustrated on Figure 3-2 where X refers to useful data and C reserved data.

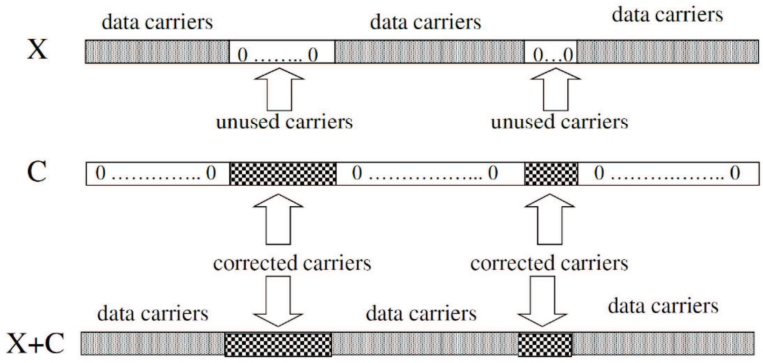

Figure 3-2: Illustration of TR method.

The performance of this technique depends on the number, the location and power of these reserved tones. While increasing the number of reserved tones improves the capability of PAPR reduction, the throughput proportionally reduces because of reduction in data bearing subcarriers. Consequently, since these dedicated tones are not used for data transmission, spectral efficiency will naturally decrease. Therefore, there is a trade-off to find between the PAPR reduction and the spectral efficiency. For example, there are 12 tones out of 64 which are unused in WLAN standard and can be employed to reduce PAPR of the OFDM modulated standard. Besides, several broadcasting standards such as DVB for Next Generation Handheld (DVB-NGH), the DVB-T2, and the recent version of Advanced Television Systems Committee Advanced Television Systems Committee (ATSC) 3.0 adopted the tone reservation as a PAPR reduction technique. Generally, in these broadcasting standards, only 1% of the subcarriers is dedicated to the PAPR reduction. For example, in the 32K mode of DVB-T2, which is today

the most deployed mode by the terrestrial broadcasting, 288 tones out of 27265 active tones are used for the PAPR reduction. The advantages of tone reservation include that there is no need neither for side information nor for special receiver oriented operation. While promising, up to the best of our knowledge tone reservation is not implemented in most of DVB-T2 transmitters, because the performance observed with TR algorithms proposed in the DVB-T2 standard do not offer a good performance-complexity trade-off.

3.1.3.3 Active Constellation Extension

ACE was introduced by Krongold and Jones in [KJ03] based on a Projection-Onto-Convex-Sets (POCS) approach to extend the outer points of a given constellation and then minimize the PAPR. In 2003, Krongold and Jones proposed a simple implementation of the ACE for faster PAPR reduction which paved the way for ACE in modern telecommunication standards. ACE is now adapted to the European Computer Manufacturers Association (ECMA) standard that specifies an Ultra-Wideband UWB physical layer (PHY-UWB) for Wireless Personal Area Network (WPANs). In addition, like TR, ACE is proposed as an optional PAPR reduction technique for the DVB-T2, DVB-N5H and ATSC 3.0.

The basic principle of the scheme is easily explained by the following example of 16-QAM constellation shown in Figure 3-3. The constellation point at the boundaries can be freely moved in the shaded region. Likewise, the other outer points can be dynamically extend away from the original constellation point. Consequently, additional co-sinusoidal and/or sinusoidal signals are added to the transmitted signal. Hence, these signals are used to reduce the time-domain peaks in the transmitted signal by intelligently adjusting the new constellation points. The advantages of ACE are that no side information is needed and the BER performance and data rate are not affected. However, this comes at the cost of a moderate increase of the power of the transmitted signal. In addition, ACE has poor performance when the number of constellation points increases as the percentage of points that can be manipulated decreases.

3.1.4 Criteria to select a PAPR reduction method

Given the large number of PAPR reduction techniques proposed in the literature the last fifteen years, it seems relevant to propose some metrics that evaluate their performance. The very first one is its PAPR reduction capability which is most of the time evaluated through out its complementary cumulative distribution function (CCDF). The larger CCDF gain, the better the PAPR reduction method. Nevertheless PAPR gain is not the single parameter that has to be taken into account. Here are some metrics that have to be considered.

3.1.4.1 Average Power reduction

Some PAPR reduction techniques result in a decrease or an increase of the average power of the transmitted signal. For example, the average power of the transmitted signal decreases when clipping is applied, while using tone reservation or active constellation extension the average power increases. As a consequence, the variation in average power denoted by δE can be defined as $\delta E = P_x - P_y$ where P_x and P_y are the

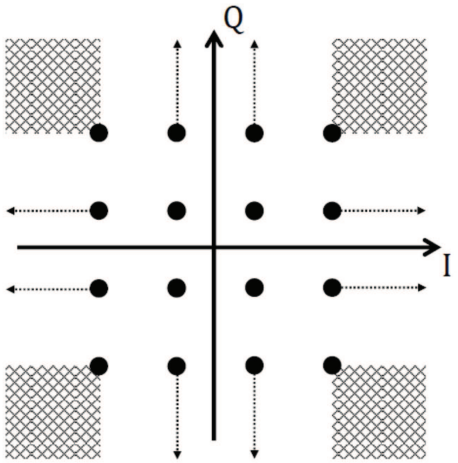

Figure 3-3: Illustration of ACE method.

average power of the signal before and after PAPR reduction, respectively. In the literature, most studies of PAPR reduction techniques performance do not take into account the average power variation of the transmitted signal. Yet this variation has a strong impact on the quality of the transmission.

3.1.4.2 In and Out of band regrowth

Some PAPR reduction techniques introduce in-band and/or out-of-band distortions because of their nonlinear characteristics. The in-band distortion is measured by the Error Vector Magnitude (EVM), while the out-of-band distortion is measured by the Adjacent Chanel Power Ratio (ACPR). These critical metrics are common figures of merit used to evaluate the quality of communication systems. Indeed, most of wireless communication standards such as the IEEE802.11a standard, the IEEE802.16e, WiMAX standard, and the LTE standard have already specified their requirements in terms of EVM and ACPR. Indeed, PAPR reduction techniques can be also categorized in two groups. The first group which causes distortions like clipping. On the other hand, the second group includes the techniques which do not introduce any distortion like tone reservation, coding, and selective mapping.

3.1.4.3 Downward compatibility

A PAPR reduction technique is said to be downward compatible if it does not imply any change on the receiver side. This is the case of tone reservation and clipping technique. However, coding, selected mapping and partial transmit sequence are not downward compatible as they require post processing on the receiver side. In fact, this characteristic is very important in both mobile and broadcast communications if a method is implemented at the transmitter side (base station).

3.1.4.4 Complexity

Even though a method has powerful characteristics, for implementation on real systems computational complexity must be taken into account. In these circumstances, too much complex techniques will be impossible to implement. Therefore, there is a trade-off between the performance and complexity of the PAPR reduction technique which must be carefully considered.

3.1.4.5 Data rate loss

The receiver, using some methods, needs additional information (side information) in order to recover useful data which degrades the capacity of the system. These methods need an increase of the bandwidth and consequently a decrease of the spectral efficiency. If the bandwidth has to be kept constant, this information transmission involves a data rate loss. This is the case of the selective mapping technique.

3.1.5 Synthesis

So far a huge number of PAPR reduction methods have been proposed for OFDM-like signals with their benefits and drawbacks. In WONG5 project, three PAPR reduction methods have been investigated for post-OFDM signal : Selected Mapping, Tone Reservation and pre-coding. This will be covered in the following sections.

3.2 Proposed methods

3.2.1 Selected Mapping

3.2.1.1 Theoretical principle

Selective Mapping (SLM) is a probabilistic technique, for reducing the Peak to Average Power Ratio (PAPR) of Multi-Carrier-Modulation signals. SLM was introduced in [BFH96] by Bauml, Fischer and Huber, where the term "selected mapping" was coined. SLM takes advantages of the fact that the PAPR of an OFDM signal is heavily dependent on phase shifts in its frequency-domain. Firstly, we generate V complex phase rotation vectors $\mathbf{C}^v$, for $0 \leq v \leq V-1$, of length N as:

$$\mathbf{C}^v = \begin{cases} (1,...,1)^{\mathsf{T}}, & v = 0, \\ (C_0^v,...,C_{N-1}^v)^{\mathsf{T}}, & 1 \leq v \leq V-1. \end{cases} \tag{3.1}$$

where, C_n^v is the n^{th} element of $\mathbf{C}^v$ defined as

$$C_n^v = e^{j\psi_k} \in \mathbb{C},\ 0 \leq v \leq V-1,\ 0 \leq n \leq N-1 \tag{3.2}$$

where, ψ_n is a uniformly distributed phase between 0 and 2π. The frequency-domain input symbols $\mathbf{X}$ with N tones, are phase rotated by V phase rotations vectors $\{\mathbf{C}^v\}_{v=0}^{V-1}$, having a size of N

$$\mathbf{X}^v = \mathbf{X}\ \odot\ \mathbf{C}^v,\ 0 \leq v \leq V-1 \tag{3.3}$$

where, $\odot$ denotes carrier-wise point-to-point multiplication. $\{\mathbf{X}^v\}_{v=0}^{V-1}$ carry same information and possess identical constellation as $\mathbf{X}$. A generic transmission scheme of a

Table 3-1: SLM parameters

V	$\in \{2, 4, 8, 16, 32\}$
C_k^v	$\in \{+1, -1, +j, -j\}$

Multi Carrier Modulation (MCM) in presence of SLM method is given by figure 3-4. In this figure, the MOD operation corresponds to a modulation operation with one of the selected WFs.

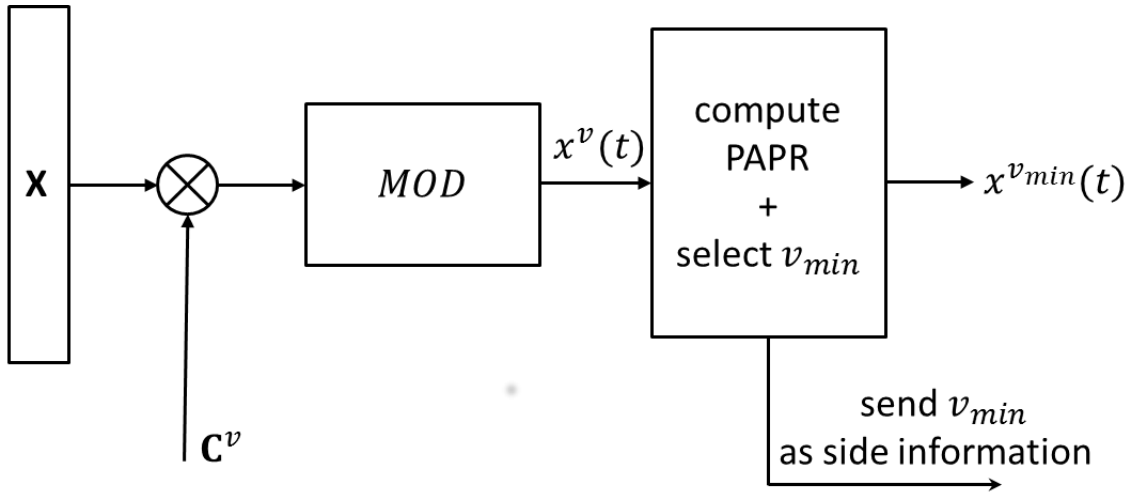

Figure 3-4: Illustration of the Tx side of an MCM scheme in presence of SLM processing.

By applying a modulation operation on $\{\mathbf{X}^v\}_{v=0}^{V-1}$, we obtain the V time-domain signal patterns $\{x^v(t)\}_{v=0}^{V-1}$. The target of the optimization problem is to identify the signal $x^{v_{min}(t)}$ that has the least PAPR so that

$$v_{min} = \underset{0 \leq v \leq V-1}{\arg\min} \Big[PAPR(x^v(t)) \Big], 0 \leq t < \infty \tag{3.4}$$

The index of respective phase rotation vector, v_{min} is sent to the receiver as side information (SI) comprising of $\log_2 V$ bits. One of the advantages of SLM technique is that it doesn't impact the BER. This technique performs PAPR reduction by generating V *independent* mappings of the time-domain signal $x(t)$ and picking the signal with lowest peak.

3.2.1.2 Simulation results

In this section, we will analyze the performance of the SLM technique over the selected post-OFDM WFs, by taking CP-OFDM as basis of comparison.

Simulation parameters The SLM parameters are given by table 3-1. While, the parameters related to each selected WF are given by table 3-2. All the simulations were carried with $16 - QAM$ modulated data symbols, over $N = 256$ subcarriers.

As depicted in table 3-1, 5 values of the parameter V have been chosen in order to study the impact of this parameter over the PAPR reduction performance. The components of each vector $\mathbf{C}^V$, $V = 2, 4, 8, 16, 32)$ are chosen in the set $\{+1, -1, +j, -j\}$.

The simulation parameters of the selected WFs are gathered in table 3-2.

Case of CP-OFDM, WOLA-OFDM, UFMC and f-OFDM In figures 3-5, 3-6, 3-7 and 3-8, we show the performance of the SLM algorithm for the modulation CP-OFDM, WOLA-OFDM, UFMC and f-OFDM. We can conclude, from these figures, that the performance in terms of PAPR reduction, increases with the number of rotation vectors V.

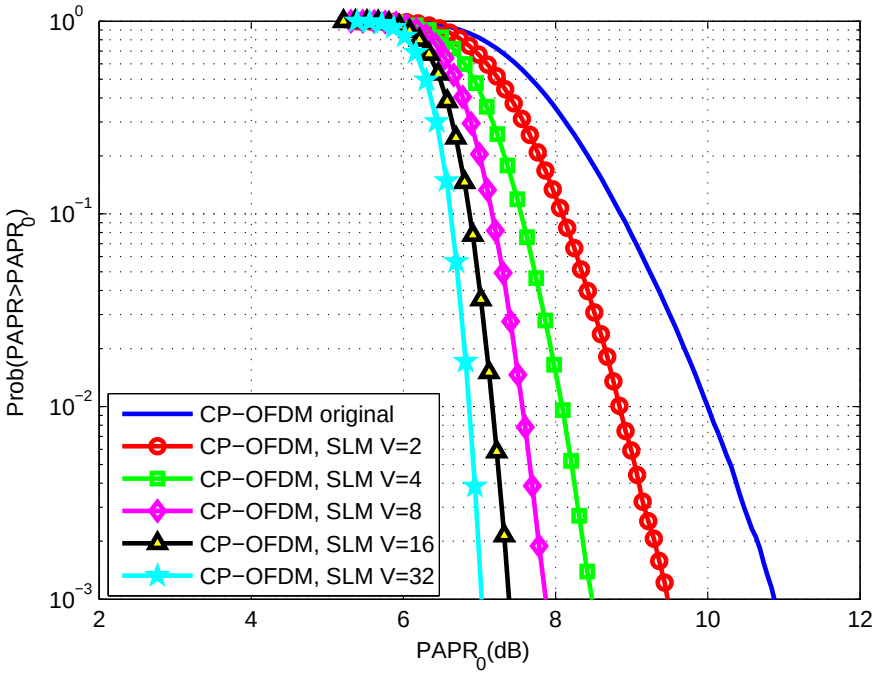

Figure 3-5: CCDF of PAPR for CP-OFDM with SLM technique and parameters of tables 3-1 and 3-2

Case of BF-OFDM For the BF-OFDM, the parameters, in table 3-2, have been chosen in order to have a 256 active subcarriers at the receiver side, which makes possible comparison of this modulation to the other studied WFs. Figure 3-9 presents the results in terms of PAPR ccdf when the PAPR is computed symbol by symbol, i.e. without considering the overlap between BF-OFDM time domain symbols.

Nevertheless, because the BF-OFDM transmitter has an embedded filter bank, there will be an overlap between the emitted symbols. The overlapping effect of two consecutive symbols in the time domain will destroy the PAPR: in fact, by overlapping two successive symbols, high peaks can be created. Figure 3-10 illustrates this problem.

Figure presents the results in terms of CCDF of the PAPR, when the PAPR is computed considering the overlap between BF-OFDM time domain symbols. We can see that there is a degradation of the PAPR due to the overlapping of BF-OFDM symbols. This degradation is similar to what has been observed for other filter banks based multicarrier modulations like FBMC-OQAM [Bul16]. Techniques proposed for FBMC-OQAM : such as "Trellis-based SLM" [BSR16b], should be adapted to BF-OFDM, in order to

Table 3-2: WFs simulation parameters

CP-OFDM	
FFT size (N)	256
CP length	18
WOLA-OFDM	
FFT size (N)	256
CP length	18
Windowing	Raised cosine
Window length (W_{Tx},W_{Rx})	$(5, 5)$
UFMC (UF-OFDM)	
FFT size (N)	256
Filter	Dolph-Chebyshev
Filter length ($\mathrm{L_{FIR}}$ =ZP+1)	19
Zero padding length	18
Stop-band attenuation	40 dB
Receive windowing	Raised cosine
f-OFDM	
FFT size (N)	256
Filter	the same at both Tx and Rx sides see D2.1 [pro16]
Filter length (L)	128
CP length (N_{CP})	18
Transition band	$2.5 \times 15\ kHz$
Burst truncation	$CP/2$ on each side
BF-OFDM	
Number of subcarrier groups (M)	32
Number of subcarrier per group ($N_{BF}/2$)	8
Rx FFT size ($MN_{BF}/2$)	256
Guar Interval, CP size	4
Transition band	$2.5 \times$ 15 kHz
Prototype Filte (for Tx filter bank)	Gaussian ($BT = 0.33$)

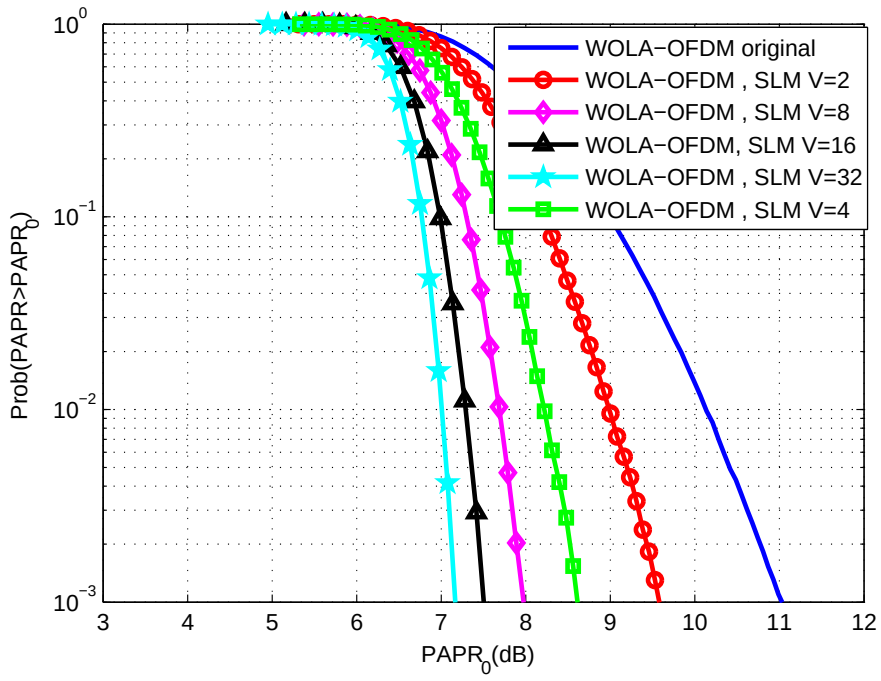

Figure 3-6: CCDF of PAPR for WOLA-OFDM with SLM technique and parameters of tables 3-1 and 3-2

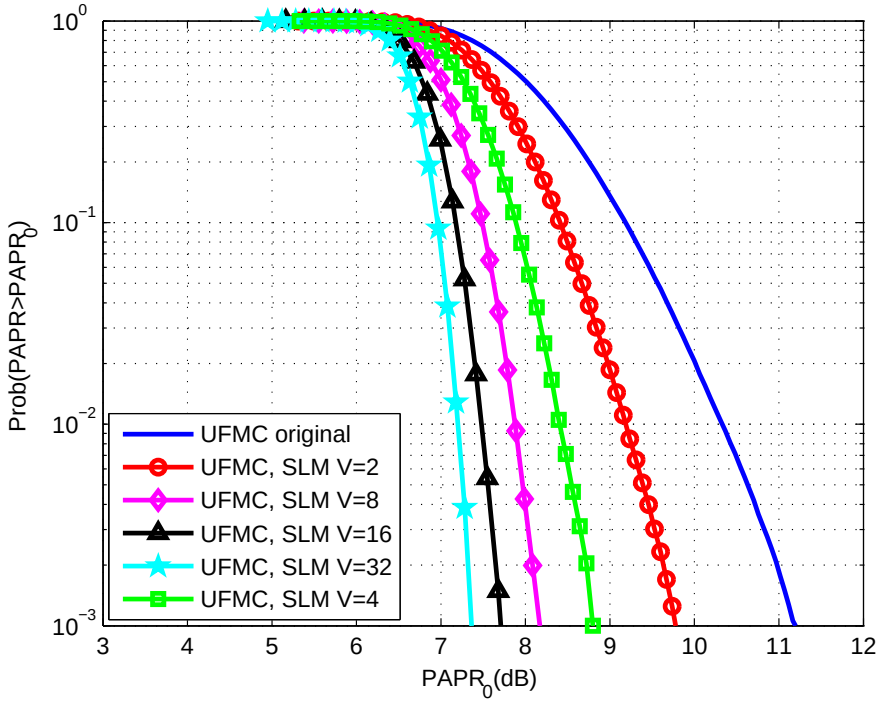

Figure 3-7: CCDF of PAPR for UFMC with SLM technique and parameters of tables 3-1 and 3-2

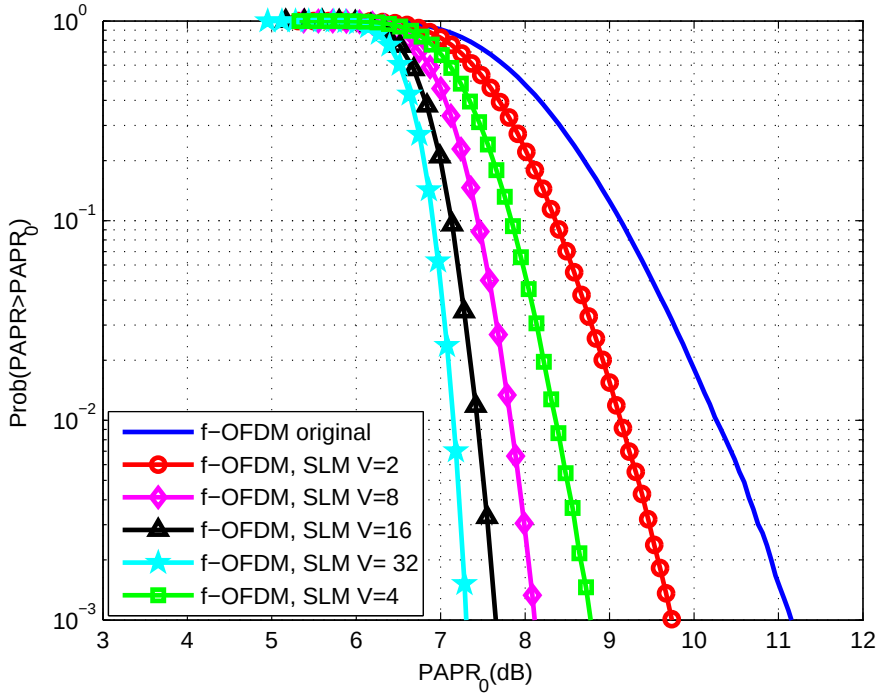

Figure 3-8: CCDF of PAPR for f-OFDM with SLM technique and parameters of tables 3-1 and 3-2

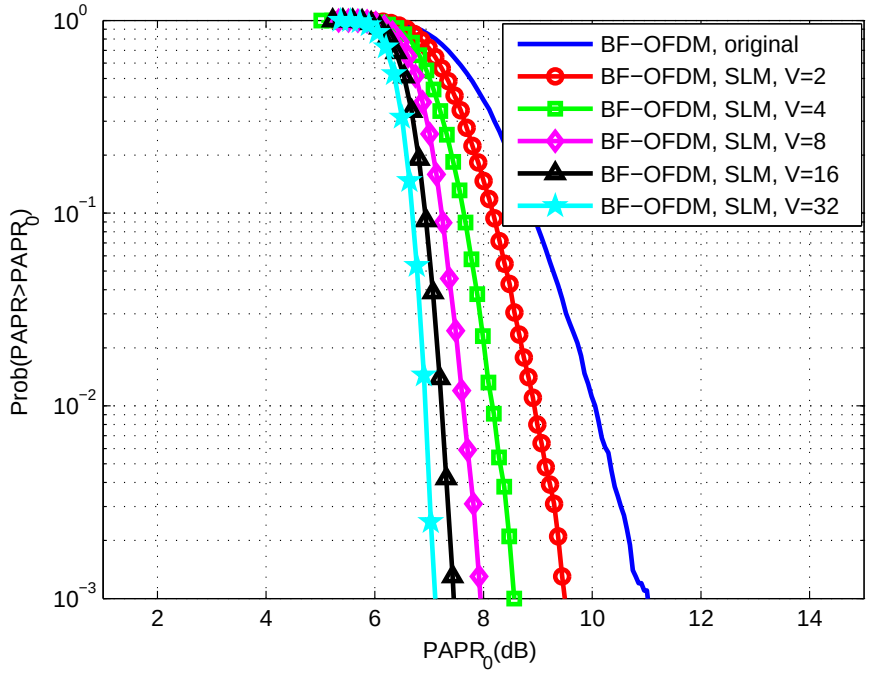

Figure 3-9: CCDF of PAPR for BF-OFDM with SLM technique and parameters of tables 3-1 and 3-2 **without considering overlap**

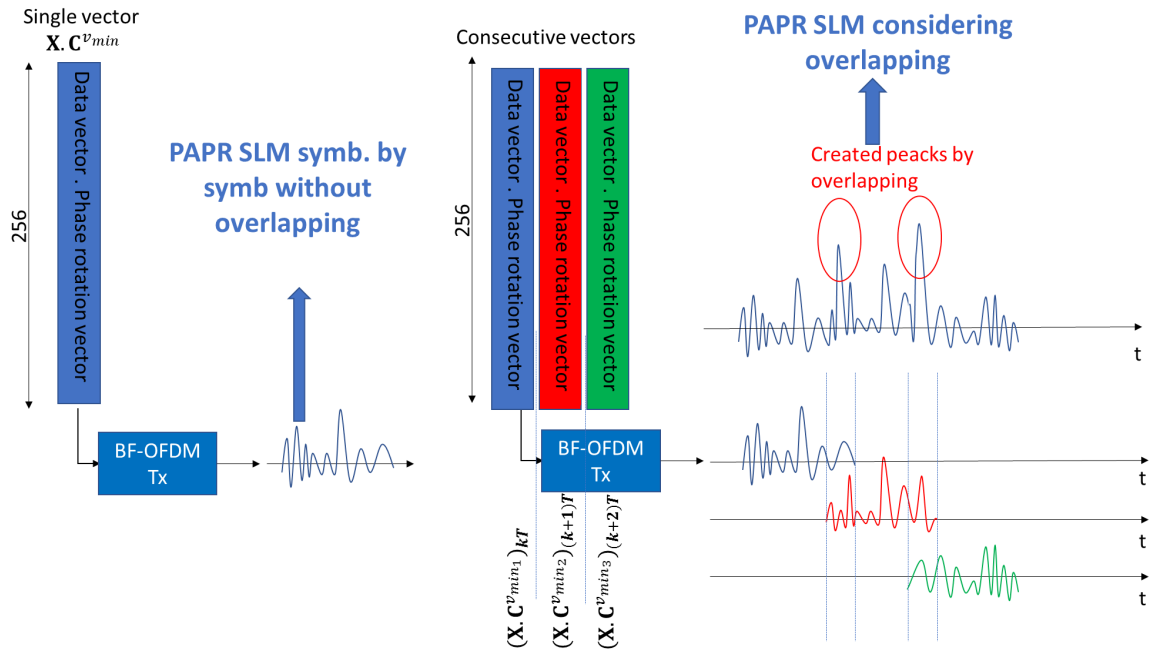

Figure 3-10: Potential problem of SLM algorithm when considering overlap between symbols in the time domain

bring the performance , in terms of PAPR reduction, close to that achieved by the other WFs.

Comparative analysis of the performance achieved by SLM technique Figure 3-12 shows the performance of the selected WFs: CP-OFDM, WOLA-OFDM, UFMC, f-OFDM and BF-OFDM with 256 subcarriers. It is seen that without PAPR reduction these waveforms have a slightly higher PAPR than the OFDM. The reason behind this differences is related to the fact that the average power of post-OFDM modulated symbols, is lower to that of CP-OFDM, due to the windowing and/or filtering applied at the transmitter side. A detailed explanation of this problem is given in deliverable D3.1 of the WONG5 project [pro17b].

With the use of the conventional SLM method the PAPR will decrease by the same amount for CP-OFDM, WOLA-OFDM, UFMC, f-OFDM. It should be noted that for large values of V, the evolution of the gain brought by SLM method becomes smaller, as confirmed by the result of table 3-3. In this table, we have reported the values of the PAPR at 10^{-3} of CCDF, corresponding to the CP-OFDM (figure 3-5). This remark remains valid for WOLA-OFDM, UFMC and f-OFDM.

Table 3-3: PAPR at 10^{-1} of CCDF for CP-OFDM (figure 3-5)

V	0	2	4	8	16	32
PAPR (dB)	$10,85$	$9,46$	$8,48$	$7,87$	$7,39$	$7,02$
Gain (dB)	0	$1,39$	$2,37$	$2,98$	$3,46$	$3,83$

However, due to the overlapping nature of the BF-OFDM time-domain symbols, the PAPR reduction achieved by the SLM algorithm is less significant with this WF. This gap

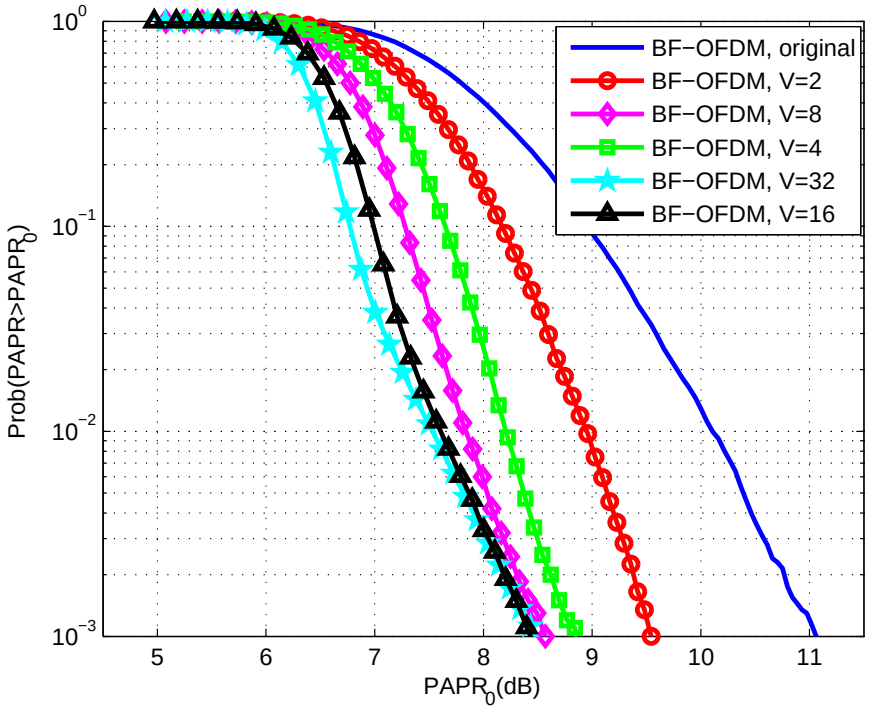

Figure 3-11: CCDF of PAPR for BF-OFDM with parameters of tables 3-1 and 3-2, when considering symbols overlapping

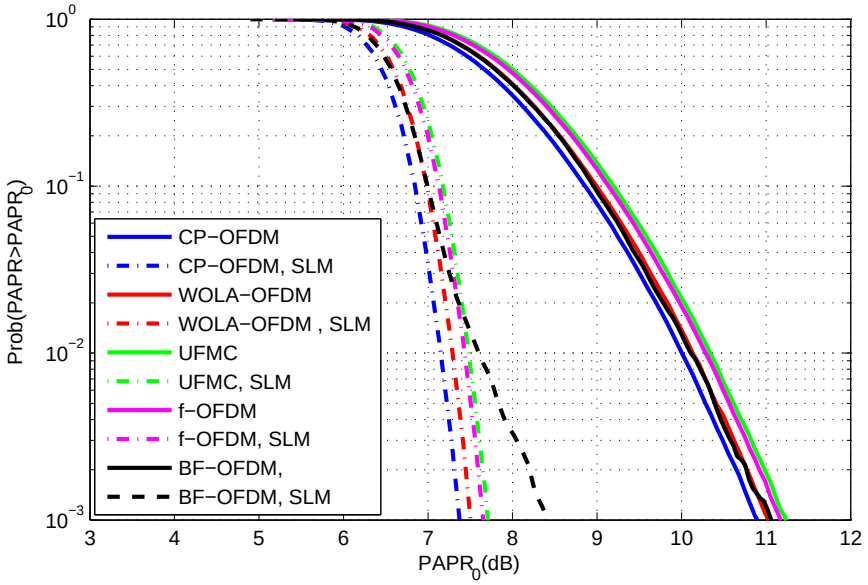

Figure 3-12: CCDF of PAPR for the selected WFs with parameters of table 3-2, $N = 256$, $V = 16$ and 16QAM

could be corrected by adapting the SLM algorithm to BF-OFDM, similarly to what was done in [Bul16] for FBMC/OQAM.

3.2.1.3 Complexity

In this section, we evaluate, for each selected WF, the complexity of reducing the PAPR by using the SLM algorithm descried in section 3.2.1.1. The complexity will be assessed by computing the number of complex multiplications needed to perform reduce the PAPR of a complex data symbol $\mathbf{X}$. In this section, we have preferred to assess the number of multiplications, per symbol, rather than per unit of time, as conducted in section 4.5 of deliverable D2.2 [pro17a].

CP-OFDM For each multiplicative vector C^v of the SLM method (V vectors) we have:

1. Multiplication of active subcarriers by vector C^v (complex rotations by $(+1, -1, +j, -j)$:
$$C^{SLM}_{1,CP-OFDM} = N \tag{3.5}$$
2. Computation of output CP-OFDM signal in the time domain, which corresponds to the CP-OFDM Tx complexity given by:
$$C^{SLM}_{2,CP-OFDM} = \frac{N}{2}\log_2(N) \tag{3.6}$$
3. Computation of PAPR in the time domain signal requires:
$$C^{SLM}_{3,CP-OFDM} = N \tag{3.7}$$

The total complexity in terms of complex multiplications is then equal to:

$$\begin{aligned} \mathrm{C}^{\mathrm{SLM}}_{\mathrm{CP-OFDM}} &= V(C^{SLM}_{1,CP-OFDM} + C^{SLM}_{2,CP-OFDM} + C^{SLM}_{3,CP-OFDM}) \\ &= V(2N + \frac{N}{2}\log_2(N)) \end{aligned} \tag{3.8}$$

WOLA-OFDM For each multiplicative vector C^v, we achieve:

1. Multiplication of active subcarriers by vector C^v:
$$C^{SLM}_{1,WOLA-OFDM} = N \tag{3.9}$$
2. Computation of WOLA-OFDM signal in the time domain:
$$C^{SLM}_{2,WOLA-OFDM} = \frac{N}{2}\log_2(N) + 2\mathrm{W}_{\mathrm{Tx}} \tag{3.10}$$
where W_{Tx} is the Tx window length.
3. Computation of PAPR in the time domain signal requires:
$$C^{SLM}_{3,WOLA-OFDM} = N + 2\mathrm{W}_{\mathrm{Tx}} \tag{3.11}$$

The total complexity in terms of complex multiplications is then equal to:

$$\begin{aligned} \mathrm{C}^{\mathrm{SLM}}_{\mathrm{WOLA-OFDM}} &= V(C^{SLM}_{1,WOLA-OFDM} + C^{SLM}_{2,WOLA-OFDM} + C^{SLM}_{3,WOLA-OFDM}) \\ &= V(2N + \frac{N}{2}\log_2(N) + 4\mathrm{W}_{\mathrm{Tx}}) \end{aligned} \tag{3.12}$$

UFMC For each vector C^v, we have :

1. Multiplication of active subcarriers by vector C^v:

$$C_{1,UFMC}^{SLM} = N \tag{3.13}$$

2. Computation of UFMC signal in the time domain. Based on the results discussed in deliverable D2.1 [pro16], regarding the Tx complexity of this WF, we can write :

$$C_{2,UFMC}^{SLM} = Bn + B\left(N + \frac{N}{2}\log_2(n)\right) + B(N + L_{FIR} - 1) + BN\lfloor\frac{L_{FIR}}{2}\rfloor \tag{3.14}$$

We remind that, for UFMC, the data is processed at the RB level (B active Rbs out of N available). For each RB, first there is the predistortion stage with n complex multiplications. Then there is the transposition to the time domain with only n active sub carriers out of N. The IFFT is therefore mainly fed by null elements and its complexity can be reduced to $N + \frac{N}{2}\log_2(n)$ complex multiplications. The convolution with the baseband real filter (of length L_{FIR}) adds $N\lfloor\frac{L_{FIR}}{2}\rfloor$ multiplications (neglecting the rise and fall time of the convolution). Finally the upconversion to the carrier frequencies counts for $(N + L_{FIR} - 1)$ multiplications.

3. Computation of PAPR in the time domain signal requires:

$$C_{3,UFMC}^{SLM} = N + L_{FIR} - 1 \tag{3.15}$$

The total complexity in terms of complex multiplications is then equal to:

$$\begin{aligned} \mathrm{C}_{\mathrm{UFMC}}^{\mathrm{SLM}} &= V(C_{1,UFMC}^{SLM} + C_{2,UFMC}^{SLM} + C_{3,UFMC}^{SLM}) \\ &= V(Bn + B\left(2N + \frac{N}{2}\log_2(n)\right) + (B+1)(N + L_{FIR} - 1) + BN\lfloor\frac{L_{FIR}}{2}\rfloor) \end{aligned} \tag{3.16}$$

f-OFDM Each multiplicative vector C^v, needs:

1. Multiplication of active subcarriers by vector C^v:

$$C_{1,f-OFDM}^{SLM} = N \tag{3.17}$$

2. Computation of f-OFDM signal in the time domain. We can refer to equation (4.8) of deliverable D2.1 [pro16]. This complexity is given by:

$$C_{2,f-OFDM}^{SLM} = \frac{N}{2}\log_2(N) + (N + N_{CP})\lfloor\frac{L}{2}\rfloor + (N + N_{CP} + L - 1) \tag{3.18}$$

where N_{CP} is the CP length and L the filter length.

3. Computation of PAPR in the time domain signal requires:

$$C_{3,f-OFDM}^{SLM} = N + L - 1 \tag{3.19}$$

The total complexity in terms of complex multiplications is then equal to:

$$\begin{aligned} \mathrm{C}_{\mathrm{f-OFDM}}^{\mathrm{SLM}} &= V(C_{1,f-OFDM}^{SLM} + C_{2,f-OFDM}^{SLM} + C_{3,f-OFDM}^{SLM}) \\ &= V(\frac{N}{2}\log_2(N) + (N + N_{CP})\lfloor\frac{L}{2}\rfloor + (2N + N_{CP} + 2L - 2)) \end{aligned} \tag{3.20}$$

BF-OFDM We remind that, for this WF, the number of active subcarriers was fixed to $\frac{MN_{BF}}{2}$, in order to make fair comparison to other WFs. For each vector C^v, the SLM algorithm carries:

1. Multiplication of active subcarriers by vector C^v (complex rotations by $(+1, -1, +j, -j)$:
$$C^{SLM}_{1,BF-OFDM} = \frac{MN_{BF}}{2} \tag{3.21}$$

2. Computation of output BF-OFDM signal in the time domain:
$$\begin{aligned} C^{SLM}_{2,BF-OFDM} = 3B\frac{N_{BF}}{2} + 3B\frac{N_{BF}}{2}\left(1 + \log_2\left(\frac{N_{BF}}{2}\right)\right) \\ + 2KMN_{BF} + 3N_{BF}\frac{M}{2}\log_2(M) \end{aligned} \tag{3.22}$$
where B is the number of active resource blocs of $N_{BF}/2$ subcarriers. In a first approximation, the Tx complexity of BF-OFDM is twice the one of CP-OFDM. We have thus:
$$C^{SLM}_{2,BF-OFDM} \sim \frac{MN_{BF}}{2}\log_2(\frac{MN_{BF}}{2}) \tag{3.23}$$

3. Computation of PAPR of the time domain signal:
$$C^{SLM}_{3,BF-OFDM} = \frac{MN_{BF}}{2} \tag{3.24}$$

The total complexity in terms of complex multiplications is then equal to:
$$\begin{aligned} \mathrm{C}^{\mathrm{SLM}}_{\mathrm{BF-OFDM}} &= V(C^{SLM}_{1,BF-OFDM} + C^{SLM}_{2,BF-OFDM} + C^{SLM}_{3,BF-OFDM}) \\ &= V(\frac{MN_{BF}}{2}\log_2(\frac{MN_{BF}}{2}) + MN_{BF}) \end{aligned} \tag{3.25}$$

As an illustration of the previous analysis, we computed in table 3-4, the normalized complexity, with respect to CP-OFDM, of the SLM algorithm applied to WOLA-OFDM, UFMC, f-OFDM and BF-OFDM. This analysis is based on the simulation parameters of table 3-2 and is obviously independent from the number of complex phase rotation vectors V.

Table 3-4: Normalized complexity of SLM algorithm with respect to CP-OFDM

WF	CP-OFDM	WOLA-OFDM	UFMC	f-OFDM	BF-OFDM
Normalized complexity	-	$1,01$	$242,93$	$12,60$	$1,67$

It's clear from the results given by table 3-4 that SLM applied to UFMC exhibits the highest complexity as compared to WOLA-OFDM, which requires mainly the same number of complex multiplications.

3.2.2 Tone reservation

3.2.2.1 Theoretical principle

Classical Tone Reservation (TR) is an adding signal technique and was first introduced in [GP97]. The idea behind TR is to isolate energy used to cancel large peaks to a predefined set of tones, namely peak reserved tones (PRTs). These tones do not carry any useful information and are orthogonal to the data tones (DTs). This orthogonality makes recovering the data trivial. Stated mathematically, the resulting signal to be transmitted will be

$$x(t) = d(t) + c(t), 0 \leq t < \infty \tag{3.26}$$

where, $c(t)$ is the peak cancellation signal and $d(t)$ is the data signal (i.e. related to data only). $x(t)$ can be represented in frequency domain as $\mathbf{X}$ given by

$$\mathbf{X} = \mathbf{D} + \mathbf{C} \tag{3.27}$$

where the n^{th} component of the vector $\mathbf{X}$ is given by

$$X_n = \begin{cases} D_n, & n \in \mathcal{B}^c \\ C_n, & n \in \mathcal{B} \end{cases} \tag{3.28}$$

where,

- $n = 1..N$ is the carrier index,
- $\mathcal{B}$ is the set of locations of PRTs, which is of length R,
- $\mathcal{B}^c$ is complement set of $\mathcal{B}$, containing the locations of DTs and is of length $N - R$,
- D_n is DT set and $D_n = 0$, for $n \in \mathcal{B}$,
- C_n is PRT set and $C_n = 0$, for $n \in \mathcal{B}^c$.

The basic principle of the TR technique and the construction of vectors $\mathbf{X}$, $\mathbf{D}$ and $\mathbf{C}$ is shown in figure 3-13. The compute the optimal location, $\mathcal{B}$, of the PRTs, we can use the peak reduction kernel method, which has been first proposed in [Tel99].

The aim of TR scheme is to compute the optimal values of PRTs subject to:

$$c(t) = \underset{C_n \; n \in \mathcal{B}}{\arg min} \Big[PAPR(MOD^{-1}\{\mathbf{D} + \mathbf{C}\}) \Big], 0 \leq t < \infty \tag{3.29}$$

where $\mathcal{MOD}^{-1}\{.\}$ is a generic demodulation operation, corresponding to one of the WFs introduced in section 2.1. Even though the problem appears to be simple, it is difficult to solve the optimization problem given by equation 3.29. Nevertheless, the optimal $c(t)$ can be obtained by solving equation (3.29), by using convex optimization algorithms such as (Quadratically constrained quadratic programs) QCQP [TC98], (projection onto convex sets) POCS [GP97], gradient search [TC98], etc. The QCQP has the computational complexity of $\mathcal{O}(RN^2)$ and yields to the optimal result. The sub-optimal approaches such as POCS and gradient search has the computational complexity of $\mathcal{O}(N \log N)$ and $\mathcal{O}(N)$ respectively.

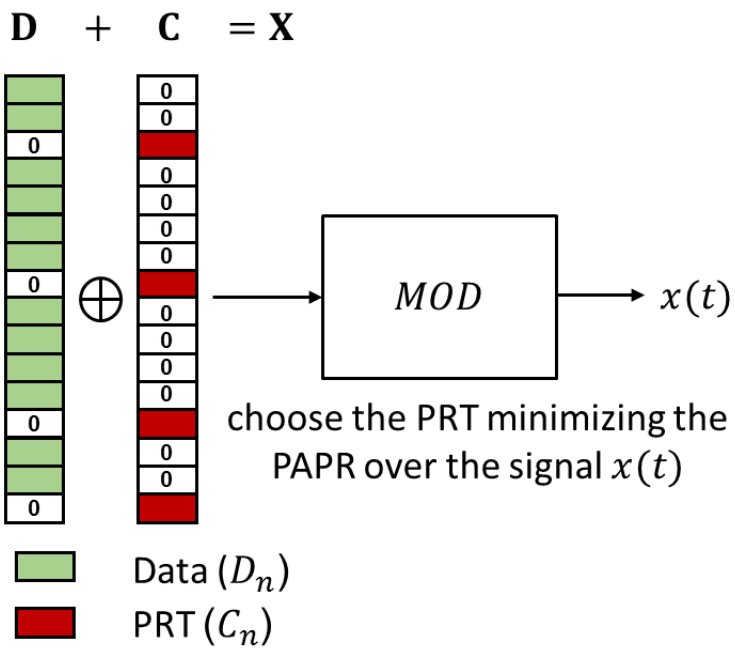

Figure 3-13: Illustration of the Tx side of an MCM scheme, in presence of TR processing.

In this work, we have used, for the computation of the PRTs, an iterative approach based the POCS algorithm and described in [GP97].

For a given data symbol vector $\mathbf{X}$, with zeros in PRT locations, we execute the steps of the following algorithm:

1. **Initialization :** Set the iteration counter k to 1.
2. **Modulation :**
   - Modulate the symbol $\mathbf{X}$, by using one of the studied waveforms.
   $$x^k(t) = \mathcal{MOD}(\mathbf{X}) \tag{3.30}$$
   - Compute the clipping threshold A^k, based on the following equation :
   $$A^k = \sqrt{PAPR_{target}\mathbb{E}\{x^k(t)^2\}} \tag{3.31}$$
   where $PAPR_{target}$ is the targeted PAPR and $\mathbb{E}\{.\}$ is the expectation operator.
3. **Peaks cancellation :**
   - Clip the modulated signal
   $$x^k_{clip}(t) = \begin{cases} x^k(t), & if \quad |x^k(t)| \leq A \\ Ae^{j\phi(x^k(t))}, & if \quad |x^k(t)| > A \end{cases} \tag{3.32}$$
   where $\phi(x^k(t))$ is the phase of the signal $x^k(t)$
   - Compute the peak cancelling signal $c^k(t)$:
   $$c^k(t) = x^k(t) - x^k_{clip}(t) \tag{3.33}$$

4. **Demodulation :** Demodulate the peak cancelling signal :

$$\mathbf{C^k} = \mathcal{MOD}^{-1}(c^k(t)) \tag{3.34}$$

5. **Reset data tones :** Reset data tones, over the vector $\mathbf{C^k}$, and update $\mathbf{X}$:

$$X_n = \begin{cases} D_n, & n \in \mathcal{B}^c \\ C_n^k, & n \in \mathcal{B} \end{cases} \tag{3.35}$$

6. **Increment or exit :**

   - if $k < N_{iter}$, where N_{iter} iterations is the maximum number of achievable iterations, $(k = k + 1)$ and reiterate steps $2 - 5$.
   - Else modulate X $(x = \mathcal{MOD}(\mathbf{X}))$ and exit.

This algorithm aims at reducing the PAPR of the signal $x(t)$, by adopting a symbol by symbol approach. A similar multi-block based approach, of this algorithms, have been applied in [Bul16] for reducing the PAPR of FBMC-OQAM signals andcould be applied to BF-OFDM.

Figure 3-14 illustrates the iterative TR algorithm, described here before, to reduce the PAPR of the waveforms considered in this deliverable.

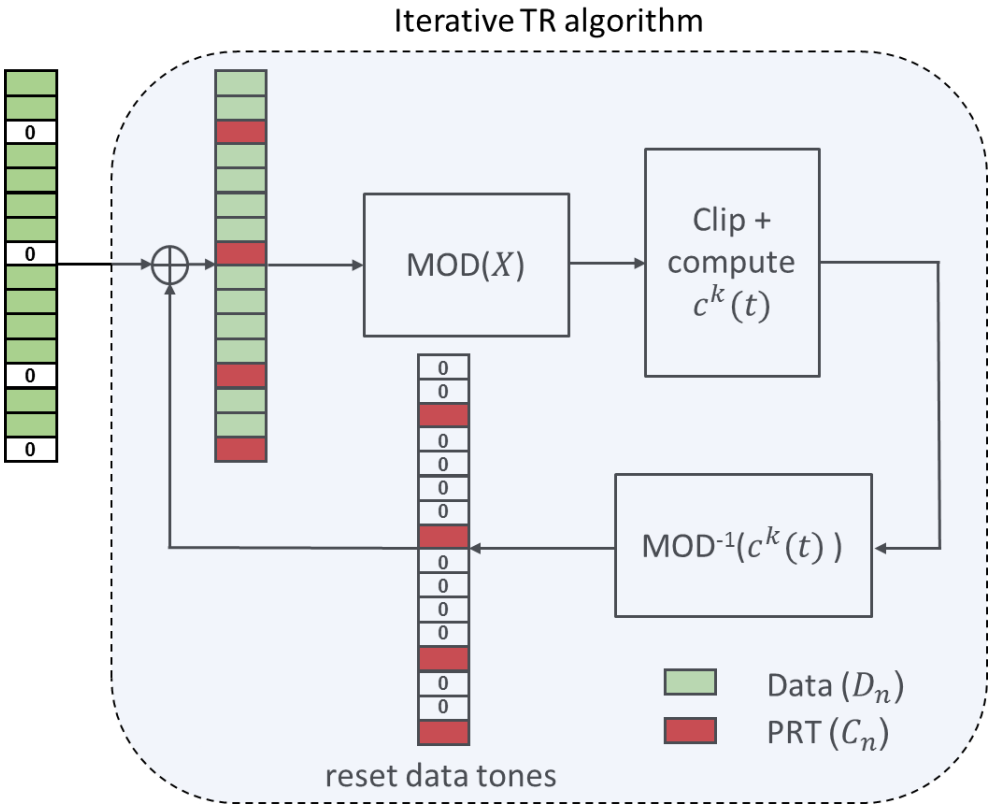

Figure 3-14: Iterative TR processing for PAPR reduction.

In TR based PAPR reduction algorithms, the reserved tones can be removed easily at the receiver side. Though impressive, TR is not without shortcomings. Since some

tones are reserved for PAPR reduction, there will induce a loss in terms of data rate. Additionally, TR technique increases the average power of the signal which means that, if more tones are to be reserved, then less power has to be allocated for PAPR reduction, which implies a tradeoff between number of reserved tones and average power increase.

3.2.2.2 Simulation results

In this section, we will study the efficiency of the adaptive TR technique, described in section 3.2.2.1, over the selected post-OFDM WFs, by taking CP-OFDM as basis of comparison. We remind that the parameters of the selected WFs are given by table 3-2. With this PAPR reduction technique, we will show the impact of tow parameters.

1. **Number of iterations :** N_{iter}, corresponding to the maximum number of achievable iterations by the adaptive TR algorithm.
2. **Ratio of Reserved Tone (RRT):** corresponding to the ration $100 \times \frac{R}{N}$. In the following, we will consider, for the RRT, the values : 5%, 8.4% and 16.8%, corresponding to 13, 21 and 42 reserved sub-carrier over 256.

The parameters related to the TR algorithm are summarized in table 3-5

Table 3-5: TR parameters

$PAPR_{target}$	4 dB
N_{iter}	$\in \{1, 5, 10, 20, 30\}$
RRT	$\in$ {5%,8.4%,16.8%}

As depicted in table 3-5, 5 values of K_{iter} have been chosen in order to study the convergence of the TR algorithm. The RRT parameters, will help us in understanding the impact of R over the PAPR reduction performance.

Case of CP-OFDM, WOLA-OFDM, UFMC and f-OFDM Figures 3-15, 3-16, 3-17 and 3-18 shows the distribution of PAPR by the TR method with $N = 256$, $QAM - 16$, $PAPR_{target} = 4dB$ with a $RRT = 5\%$ and for different iteration numbers. It is clearly seen, from this figure, that the performance, in terms of PAPR reduction, increases with the number of iterations, especially between 1 and 20 iterations. After 20 iterations, the gain, in terms of PAPR reduction, becomes smaller

Figures 3-19, 3-20, 3-21 and 3-22 illustrate the impact of RRT on PAPR reduction, with $N = 256$, $QAM - 16$, $PAPR_{target} = 4dB$ at 20 iterations. It can thus be seen that with the increase of the RRT, the performance in terms of the PAPR reduction becomes better for CP-OFDM, WOLA-OFDM, UFMC and f-OFDM.

Case of BF-OFDM For BF-OFDM, the number of iterations for the TR algorithm has been taken equal to 30. Figure 3.2.2.2 presents the results in terms of CCDF of the PAPR when the PAPR is computed symbol by symbol, i.e. without considering the overlap between BF-OFDM time domain symbols.

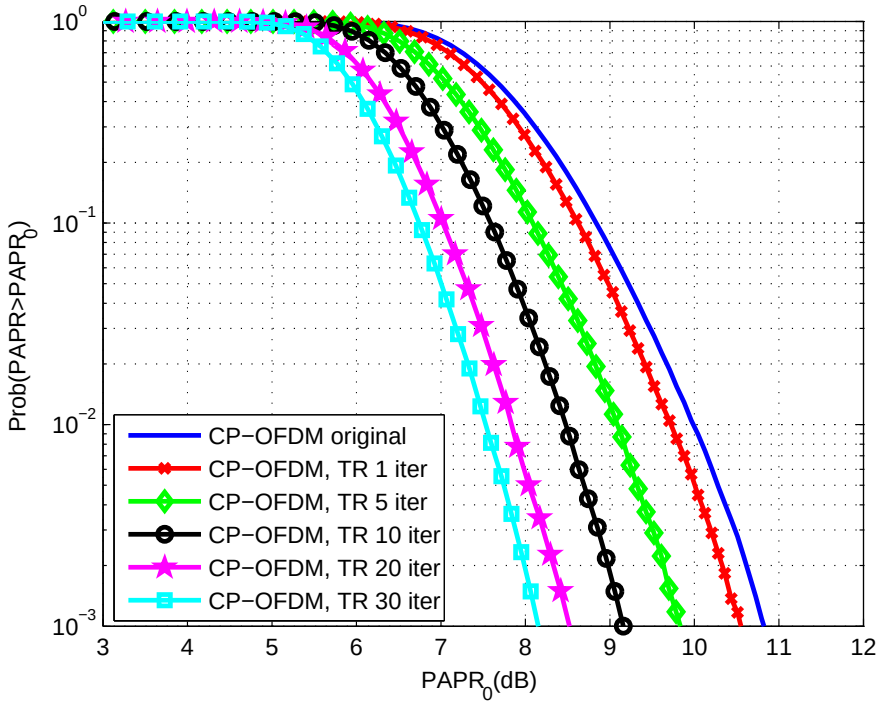

Figure 3-15: CCDF of the PAPR, for CP-OFDM, by the TR method with $PAPR_{target}$ = 4 dB, RRT = 5% and for different iteration numbers N_{iter}

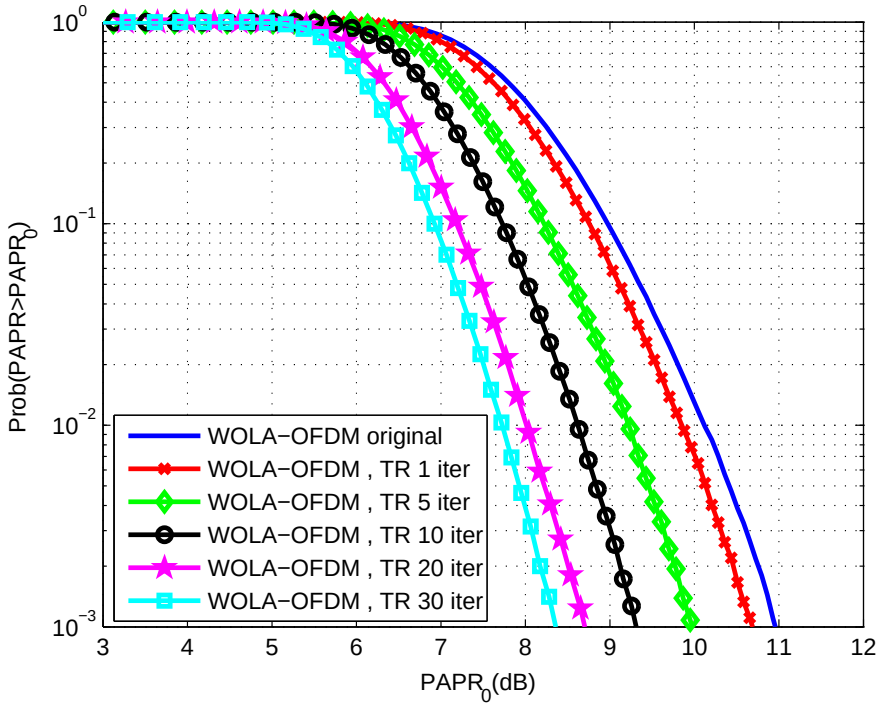

Figure 3-16: CCDF of the PAPR, for WOLA-OFDM, by the TR method with $PAPR_{target}$ = 4 dB RRT = 5% and for different iteration numbers N_{iter}

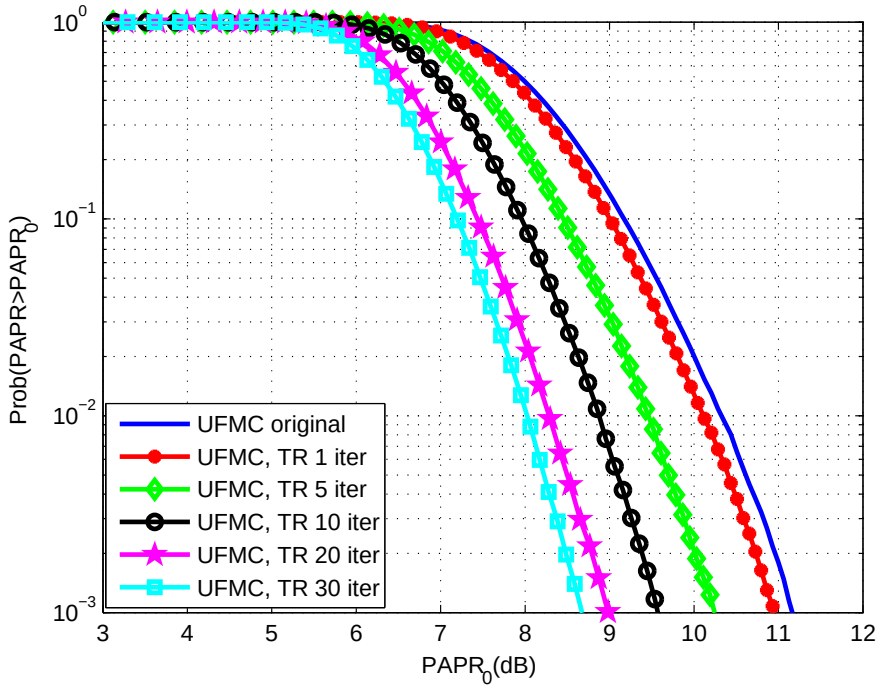

Figure 3-17: CCDF of the PAPR, for UFMC, by the TR method with $PAPR_{target}$ = 4 dB, RRT = 5% and for different iteration numbers N_{iter}

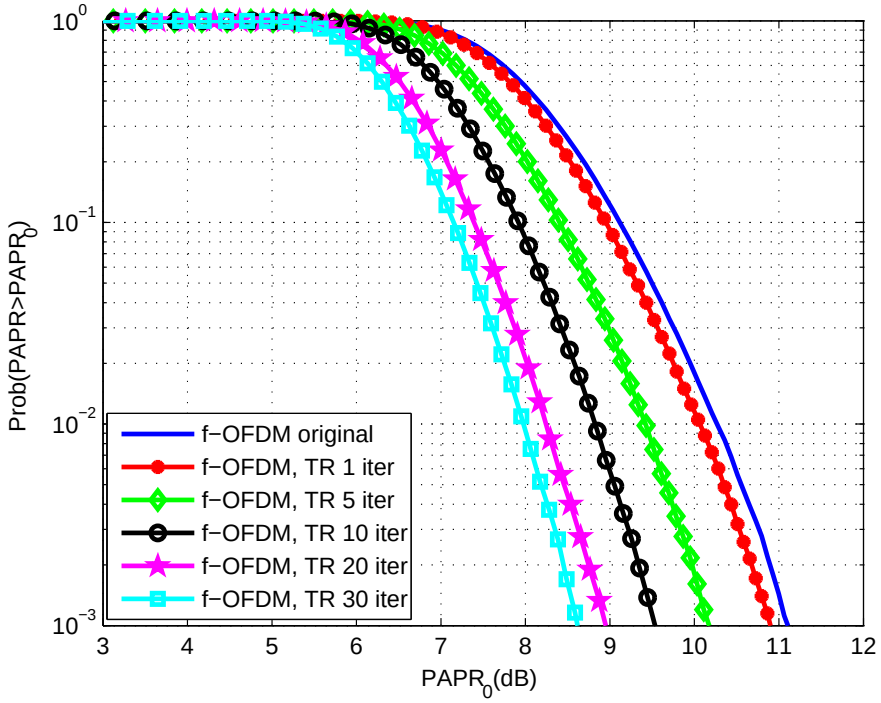

Figure 3-18: CCDF of the PAPR, for f-OFDM, by the TR method with $PAPR_{target}$ = 4 dB, RRT = 5% and for different iteration numbers N_{iter}

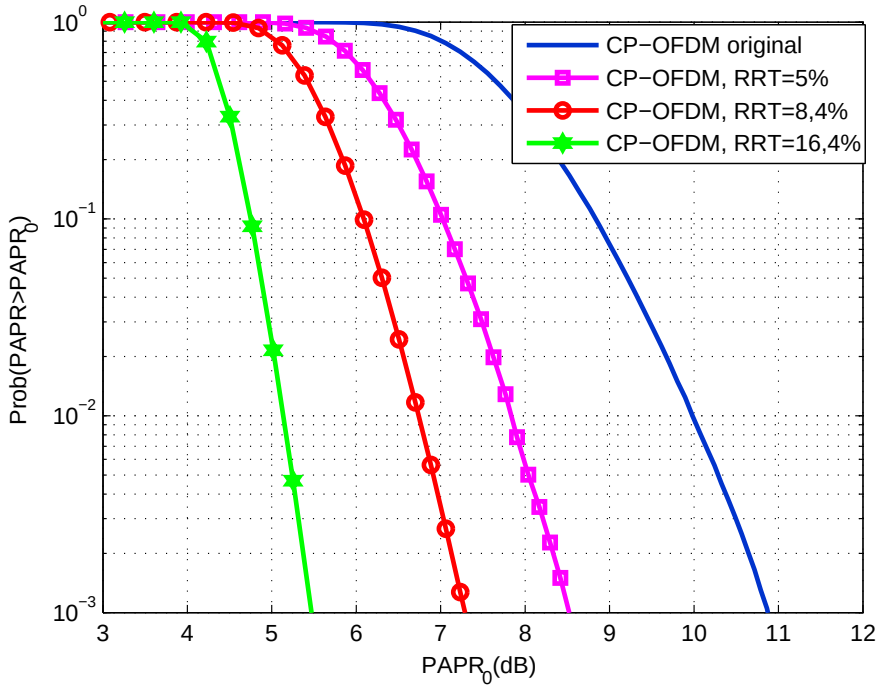

Figure 3-19: CCDF of the PAPR, for CP-OFDM, by the TR method with $PAPR_{target}$ = 4 dB, at 20 iterations and for different values of RRT

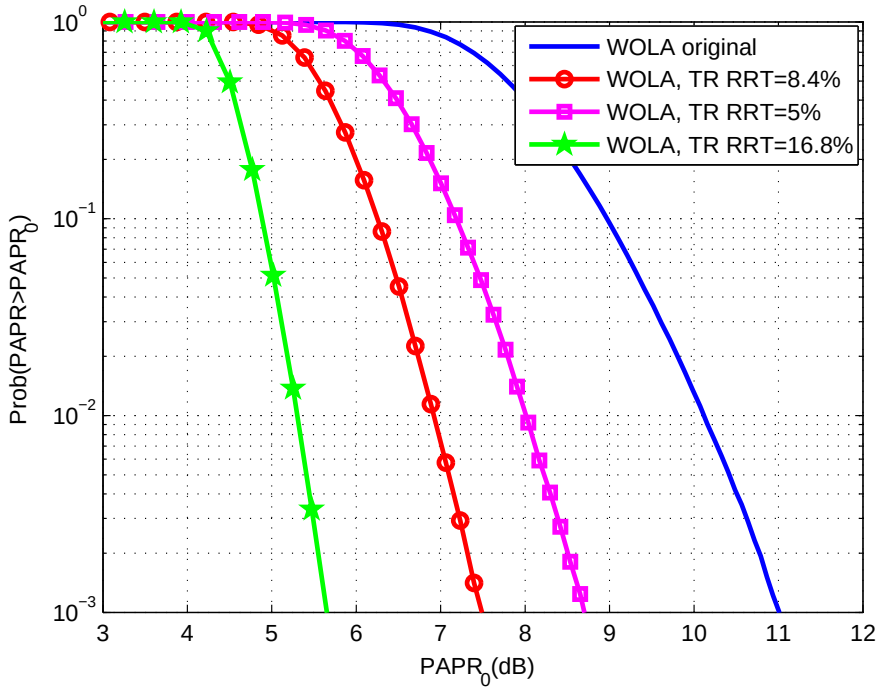

Figure 3-20: CCDF of the PAPR, for WOLA-OFDM, by the TR method with $PAPR_{target}$ = $4\ dB$, at 20 iterations and for different values of RRT

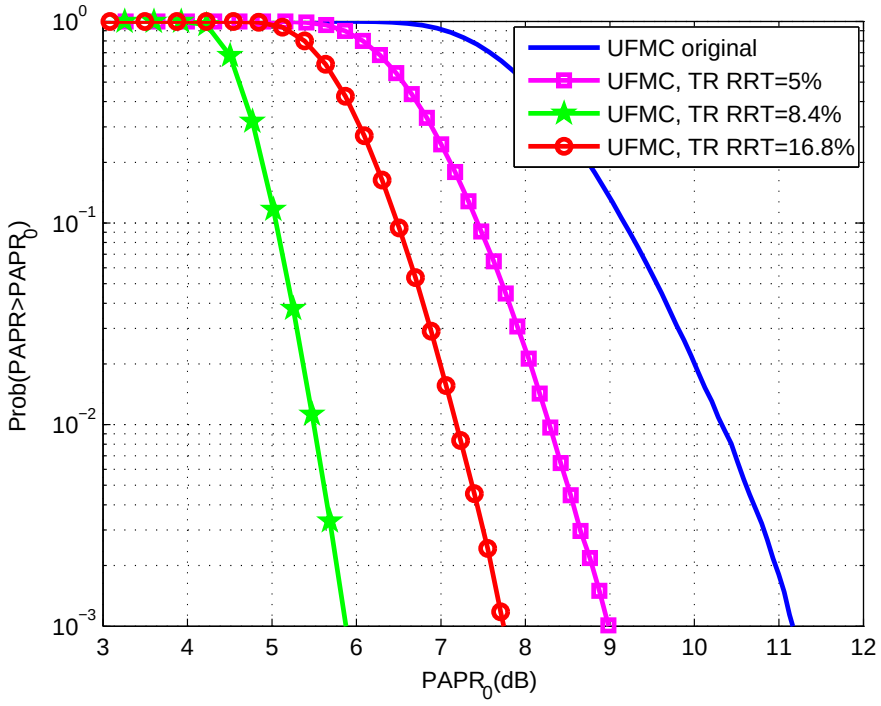

Figure 3-21: CCDF of the PAPR, for UFMC, by the TR method with $PAPR_{target} = 4\ dB$, at 20 iterations and for different values of RRT

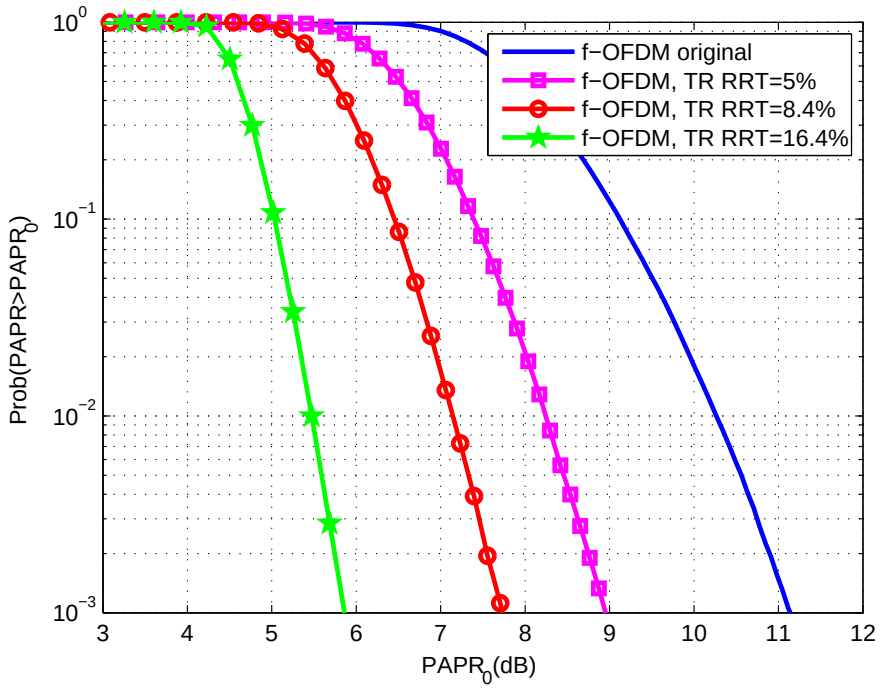

Figure 3-22: CCDF of the PAPR, for f-OFDM, by the TR method with $PAPR_{target} = 4\ dB$, at 20 iterations and for different values of RRT

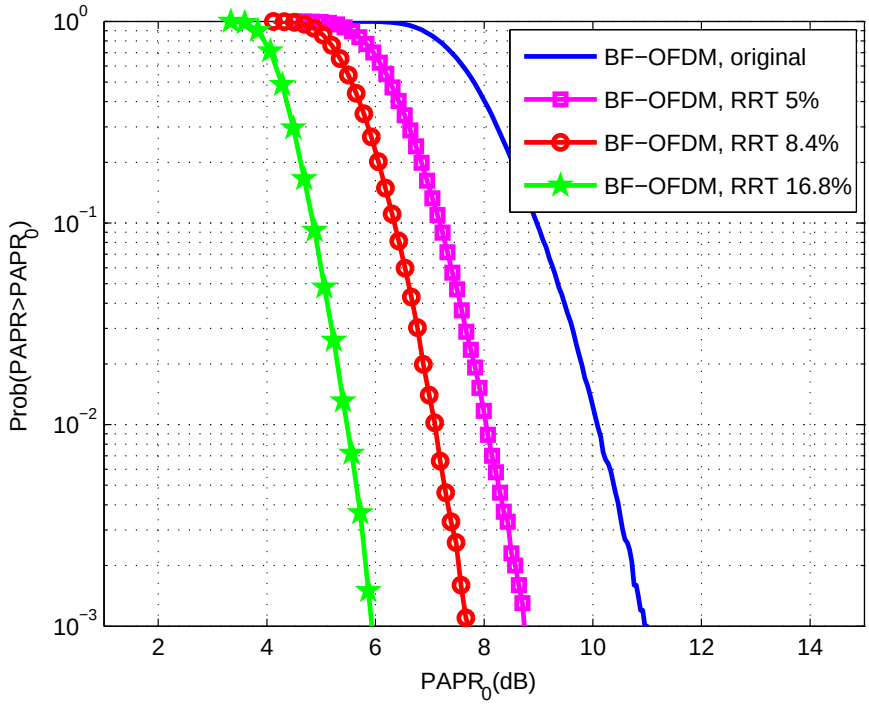

Figure 3-23: CCDF of the PAPR, for BF-OFDM, by the TR method with $PAPR_{target}$ = 4 dB, at 30 iterations, for different values of RRT, **PAPR computed without considering symbols overlap**

When the TR algorithm is applied symbol by symbol, without considering any overlap between two successive symbols, results obtained by the TR method are comparable to those obtained for other waveforms. The TR algorithm used for getting the results of figure is as follows:

1. Generate a vector, X, of 256 complex data symbols (where R tones are reserved for PAPR reduction, set to zero and cannot be used for data, only 256-R tones are used for data),
2. Generate the output BF-OFDM corresponding signal in the time domain: $x = BF_{OFDM}(X)$,
3. Compute the complex values of the reserved tones in order to minimize PAPR ($C^{N_{iter}}$ is a vector of size 256 with all data tones equal to zero and R non null reserved tones),
4. Compute the output BF-OFDM signal in the time domain with TR PAPR reduction: $x^{PAPR} = BF_{OFDM}(X + C^{N_{iter}})$,
5. Compute original PAPR and PAPR with TR method:

$$PAPR_{original} = PAPR(x) \tag{3.36}$$

$$PAPR_{TR} = PAPR(x^{PAPR}) \tag{3.37}$$

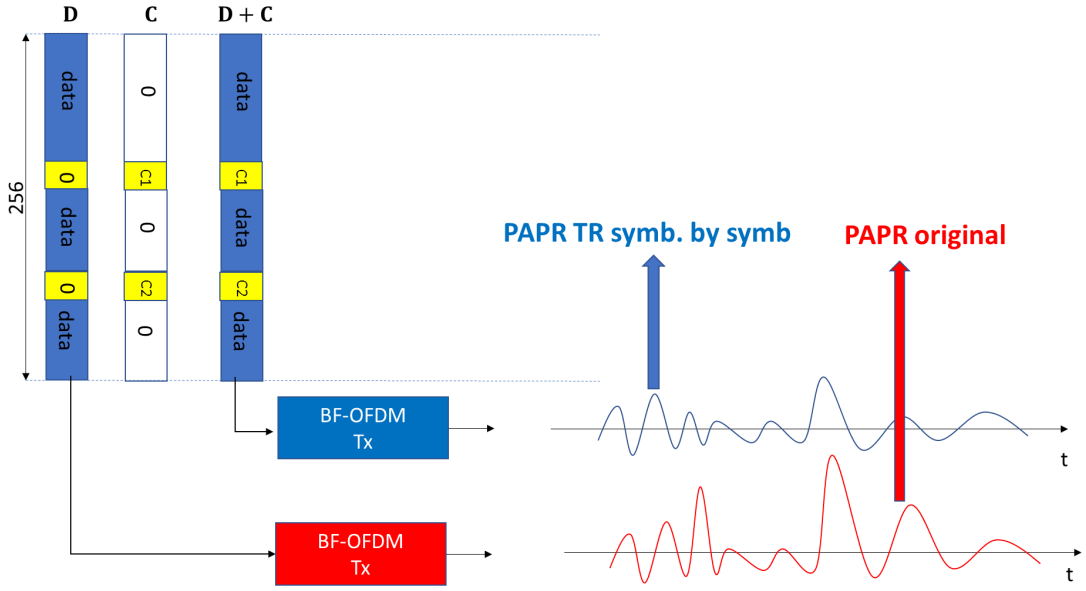

Figure 3-24: TR algorithm and PAPR computation without considering overlap

Figure 3-24 explains the TR algorithm and the PAPR computation, when the overlap between BF-OFDM, time-domain symbols is not taken into account:

Nevertheless, because the BF-OFDM transmitter has an embedded filter bank, there will be overlap between the emitted symbols. The overlapping effect of two consecutive symbols in the time domain will destroy the PAPR: in fact, by overlapping two successive symbols, high peaks can be created. Figure 3-25 illustrates this problem.

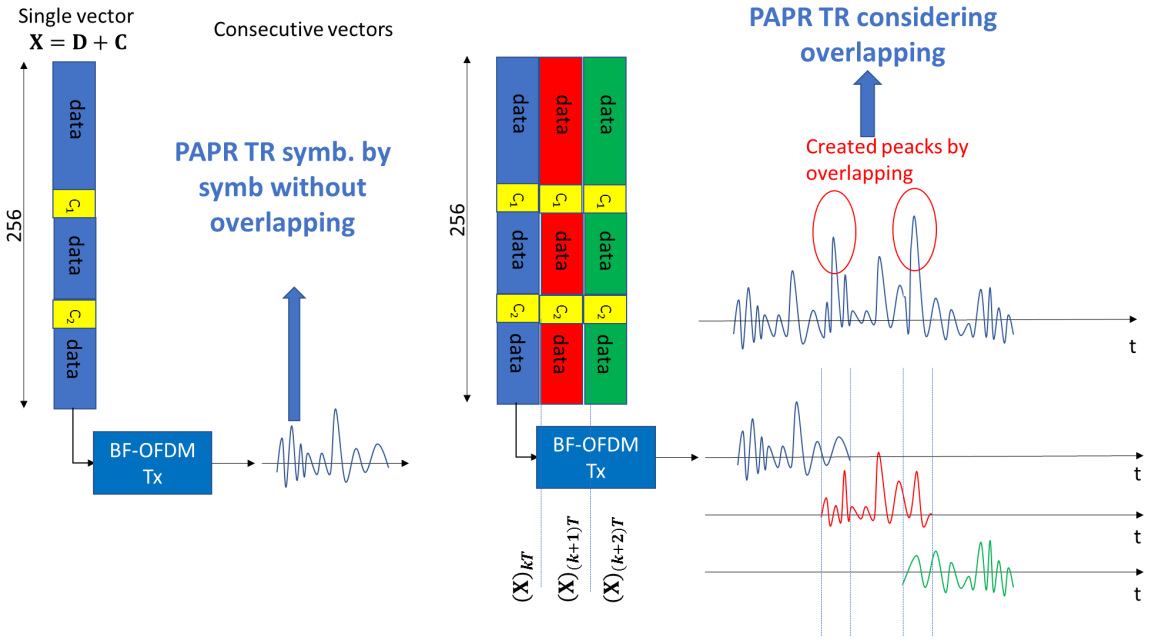

Figure 3-25: Potential problem of TR algorithm when considering overlap between symbols in the time domain

Figure 3-26 presents the results in terms of CCDF of the PAPR when the PAPR is computed considering the overlap between BF-OFDM time domain symbols. We can see that there is a degradation of the PAPR due to the overlapping of BF-OFDM symbols. This degradation is similar to what has been observed for other filter banks based multicarrier modulations like FBMC-OQAM [BSR15b]. Techniques used for FBMC-OQAM, such as "Dispersive Tone Reservation Technique" [BSR15b], could be applied to BF-OFDM.

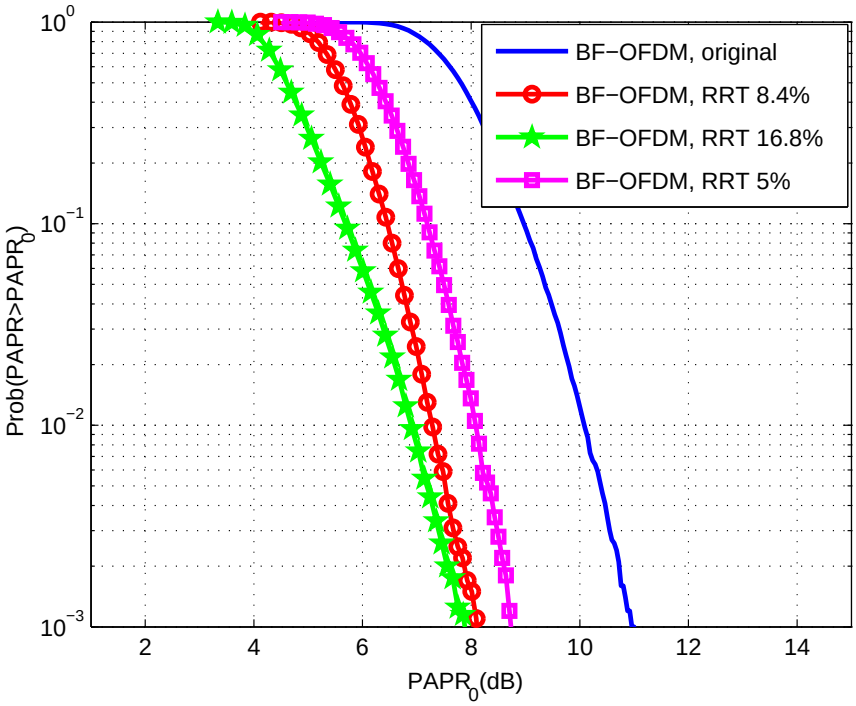

Figure 3-26: CCDF of the PAPR, for BF-OFDM, by the TR method with $PAPR_{target}$ = 4 dB, at 30 iterations, for different values of RRT, **PAPR computed considering symbols overlap**

In figure 3-27, we show in the same plot the impact of the overlapping between BF-OFDM symbols as function of the iteration numbers N_{iter} and for and $RRT = 5\%$. One can conclude, form this figure, that the past symbols impact very slightly the reduced PAPR when, not taken into account in the computation of the reserved tones for the current symbol.

Comparative analysis of the performance achieved by TR technique Figure 3-28 shows the performance of the WFs: CP-OFDM, WOLA-OFDM, UFMC f-OFDM and BF-OFDM with 256 subcarriers. The TR algorithm with $RRT = 8,4\%$, was stopped after $N_{iter} = 20$. It is seen, without PAPR reduction, that these waveforms have a slightly higher PAPR than the OFDM. As explained in section 3.2.1.2, the reason behind this differences is related to the fact that the average power of post-OFDM modulated symbols, is lower to that of CP-OFDM, due to the windowing and/or filtering applied at the transmitter side.

With the use of the conventional classical TR algorithm, the PAPR will decrease

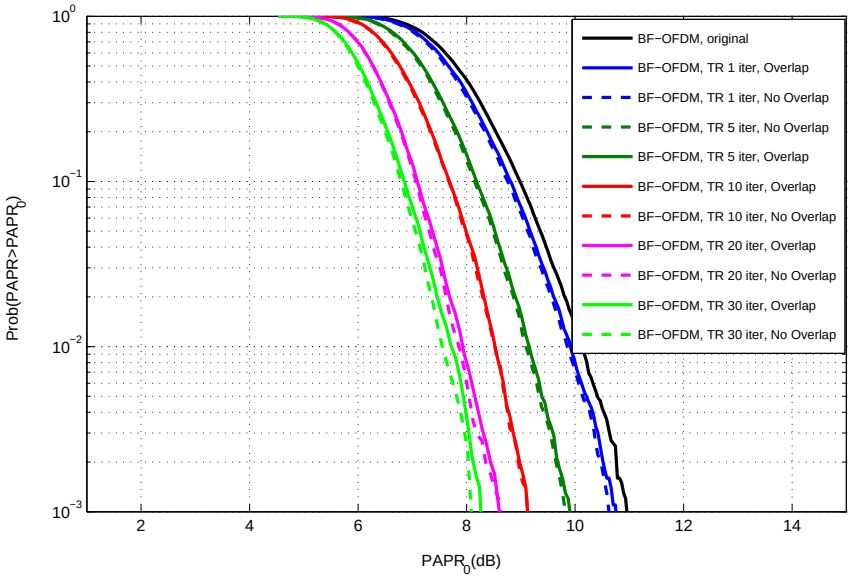

Figure 3-27: CCDF of the PAPR, for BF-OFDM, by the TR method with $PAPR_{target}$ = 4 dB, RRT = 5% and for different iteration numbers N_{iter}

by the same amount for the CP-OFDM, WOLA-OFDM, UFMC, f-OFDM. However, due to the overlapping nature of the BF-OFDM time-domain symbols, the PAPR reduction achieved by the TR algorithm is less significant. This degradation could be corrected by adapting the TR algorithm to BF-OFDM, similarly to what was done in [Bul16] for FBMC/OQAM signals.

3.2.2.3 Complexity

As carried for the SLM algorithm, we will assess, in this section, the complexity of TR algorithm adapted to all the WFs considered in this deliverable. The complexity will be computed in terms of complex multiplications, required to achieve the computation of the peak cancellation signal over N modulated data symbols.

CP-OFDM At each iteration of the TR method we have:

1. Computation of output CP-OFDM signal in the time domain. This complexity is given by equation (3.6).

$$C^{TR}_{1,CP-OFDM} = C^{SLM}_{1,CP-OFDM} = \frac{N}{2}\log_2(N) \tag{3.38}$$

2. Computation of the signal $\mathbf{C}$ in the frequency domain, equal to : $CP - OFDM^{-1}(c^k(t))$. This operation has the same complexity as a CP-OFDM receiver.

$$C^{TR}_{2,CP-OFDM} = \frac{N}{2}\log_2(N) = C^{TR}_{1,CP-OFDM} \tag{3.39}$$

The total complexity, in terms of complex multiplications, is then equal to:

$$\begin{aligned} \mathrm{C}^{\mathrm{TR}}_{\mathrm{CP-OFDM}} &= 2N_{iter}C^{TR}_{1,CP-OFDM} \\ &= N_{iter}N\log_2(N) \end{aligned} \tag{3.40}$$

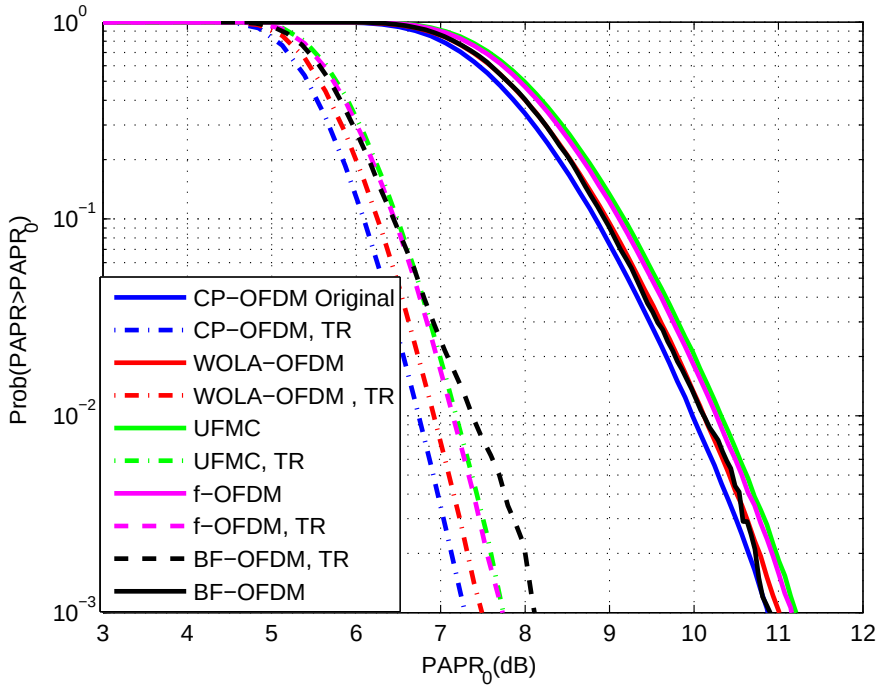

Figure 3-28: CCDF of PAPR for the selected WFs with TR algorithm and parameters of table 3-2, $N = 256$, 16QAM, $PAPR_{target}$ = 4 dB, , $N_{iter} = 20$ and $RRT = 8,4\%$

WOLA-OFDM At each iteration of the TR method we need the:

1. Computation of output WOLA-OFDM signal in the time domain. This complexity is given by equation (3.10).

$$C^{TR}_{1,WOLA-OFDM} = C^{SLM}_{1,WOLA-OFDM} = \frac{N}{2}\log_2(N) + 2\mathrm{W_{Tx}} \tag{3.41}$$

2. Computation of the signal $\mathbf{C}$ in the frequency domain, equal to : $WOLA - OFDM^{-1}(c^k(t))$. This operation has the same complexity as a WOLA-OFDM demodulator.

$$C^{TR}_{2,WOLA-OFDM} = \frac{N}{2}\log_2(N) + 2\mathrm{W_{Rx}} \tag{3.42}$$

where $\mathrm{W_{Rx}}$ is the length of the window applied at the receiver side.

The total complexity, in terms of complex multiplications, is then equal to:

$$\begin{aligned} \mathrm{C^{TR}_{WOLA-OFDM}} &= N_{iter}(C^{TR}_{1,WOLA-OFDM} + C^{TR}_{2,WOLA-OFDM}) \\ &= N_{iter}(N\log_2(N) + +2\mathrm{W_{Tx}} + 2\mathrm{W_{Rx}}) \end{aligned} \tag{3.43}$$

UFMC At each iteration, we need:

1. Computation of output UFMC signal in the time domain. This complexity is given by equation (3.14).

$$\begin{aligned} C^{TR}_{1,UFMC} &= C^{SLM}_{1,UFMC} \\ &= Bn + B\left(N + \frac{N}{2}\log_2(n)\right) + B(N + L_{FIR} - 1) + BN\lfloor\frac{L_{FIR}}{2}\rfloor \end{aligned} \tag{3.44}$$

2. Computation of the signal $\mathbf{C}$ in the frequency domain, equal to : $UFMC^{-1}(c^k(t))$. If no windowing is applied at receiver side, the complexity of this operation (equation (4.10) of deliverable D2.1 [pro16]) is equal to

$$C^{TR}_{2,UFMC} = N\log_2(2N) \tag{3.45}$$

The total complexity, in terms of complex multiplications, is then equal to:

$$\begin{aligned} \mathrm{C}^{\mathrm{TR}}_{\mathrm{UFMC}} &= N_{iter}(C^{TR}_{1,UFMC} + C^{TR}_{2,UFMC}) \\ &= N_{iter}(Bn + B\left(N + \frac{N}{2}\log_2(n)\right) + B(N + L_{FIR} - 1) + BN\lfloor\frac{L_{FIR}}{2}\rfloor + N\log_2(2N)) \end{aligned} \tag{3.46}$$

f-OFDM At each iteration of the TR algorithm, we expect:

1. Computation of output f-OFDM signal in the time domain. This complexity is given by equation (3.18).

$$C^{TR}_{1,f-OFDM} = C^{SLM}_{1,f-OFDM} = \frac{N}{2}\log_2(N) + (N + N_{CP})\lfloor\frac{L}{2}\rfloor + (N + N_{CP} + L - 1) \tag{3.47}$$

2. Computation of the signal $\mathbf{C}$ in the frequency domain, equal to : $f - OFDM^{-1}(c^k(t))$. This operation has the same complexity as a that of the transmitter side.

$$C^{TR}_{2,f-OFDM} = C^{TR}_{1,f-OFDM} \tag{3.48}$$

The total complexity, in terms of complex multiplications, is then equal to:

$$\begin{aligned} \mathrm{C}^{\mathrm{TR}}_{\mathrm{f-OFDM}} &= N_{iter}(C^{TR}_{1,f-OFDM} + C^{TR}_{2,f-OFDM}) \\ &= 2N_{iter}C^{TR}_{1,f-OFDM} \end{aligned} \tag{3.49}$$

BF-OFDM For each iteration of the TR method we have:

1. Computation of output BF-OFDM signal in the time domain. This complexity is given by equation (3.23). This complexity is twice the one of CP-OFDM

$$C^{TR}_{1,BF-OFDM} = C^{SLM}_{2,BF-OFDM} = \frac{MN_{BF}}{2}\log_2(\frac{MN_{BF}}{2}) \tag{3.50}$$

2. Computation of the signal $\mathbf{C}$ in the frequency domain, equal to : $BF - OFDM^{-1}(c^k(t))$. This operation has the same complexity as a CP-OFDM receiver.

$$C^{TR}_{2,BF-OFDM} = \frac{MN_{BF}}{4}\log_2(\frac{MN_{BF}}{2}) \tag{3.51}$$

The total complexity in terms of complex multiplications is then equal to:

$$\begin{aligned} \mathrm{C}^{\mathrm{TR}}_{\mathrm{BF-OFDM}} &= C^{TR}_{1,BF-OFDM} + C^{TR}_{2,BF-OFDM} \\ &= N_{iter}\frac{3MN_{BF}}{4}\log_2(\frac{MN_{BF}}{2}) \end{aligned} \tag{3.52}$$

Table 3-6: Normalized complexity of TR algorithm with respect to CP-OFDM

WF	CP-OFDM	WOLA-OFDM	UFMC	f-OFDM	BF-OFDM
Normalized complexity	-	$1,01$	$180,51$	$18,90$	$1,50$

To illustrate the previous analysis, we computed in table 3-6, the normalized complexity, with respect to CP-OFDM, of the proposed TR algorithm applied to WOLA-OFDM, UFMC, f-OFDM and BF-OFDM. This analysis is based on the simulation parameters of table 3-2 and is obviously independent from the number of iterations N_{iter} of the TR algorithm.

We can deduce, from the numerical values given by table 3-6, that the ranking, in terms of TR algorithm processing complexity, is the same as the one obtained with SLM. Indeed, while TR applied to WOLA-OFDM exhibits nearly same complexity as in the case of CP-OFDM, UFMC is nearly 180 times more complex.

3.2.3 Precoding-based PAPR reduction technique

3.2.3.1 Theoretical principle

A precoding technique consists in multiplying the modulated data of each UF-OFDM block by a precoding matrix before the subset assignment IDFT block. The precoding matrix is of the same size as the allocated subcarrier vector. The dimension of the precoding matrix, denoted by **P**, is, hence, $N_a \times N_a$. It is used as a spreading code and can be expressed as:

$$\mathbf{P} = \begin{bmatrix} P_{0,0} & P_{0,1} & \cdots & P_{0,N_a-1} \\ P_{1,0} & P_{1,1} & \cdots & P_{1,N_a-1} \\ \vdots & \vdots & \ddots & \vdots \\ P_{N_a-1,0} & P_{N_a-1,1} & \cdots & P_{N_a-1,N_a-1} \end{bmatrix}. \tag{3.53}$$

To simplify the reverse precoding process, the matrix **P** has to be a unitary matrix which means that $\mathbf{P}\mathbf{P}^H = \mathbf{I}_{N_a}$. Also, as the precoding is performed before the IDFT, it should contain a signal transform to the frequency domain. Hence, we obtain:

$$\mathbf{P} = [P_{ij}]_{i,j \in [\![0,N_a-1]\!]} \tag{3.54}$$

where $P_{ij} = P_{i0}e^{-\frac{2\pi ij}{N_a}}$, and $P_{i0}, i \in [\![0, N_a-1]\!]$ are the coefficients of a mother function. In this document, the rectangular is used as a mother function. We refer to the precoded UF-OFDM and F-OFDM using a rectangular filter respectively by DFT-UF-OFDM and DFT-F-OFDM.

In UF-OFDM, the data symbols $\{x_n\}_{n \in [\![0,N_a-1]\!]}$ are assigned to each subcarrier in the allocated subcarrier set, containing N_a subcarriers. Then, they are divided into B sub-sets. Each sub-set contains N_B consecutive subcarriers and consequently N_B data symbols. A N-point inverse discrete Fourier transform (IDFT) operation is performed for every sub-set to be transformed inot the frequency domain.

The proposed precoding scheme consists in multiplying the data symbols $\{x_n\}_{n\in[\![0,N_a-1]\!]}$ before subdivision into sub-sets by the precoding matrix defined in (3.54) to obtain $\{X_p\}_{p\in[\![0,N_a-1]\!]}$. Therefore, the UF-OFDM output signal can be written as $s_k = \sum_{b=0}^{B}\sum_{m=0}^{N-1}\tilde{x}_m^b f_{k-mN}^b$ where $\tilde{x}_m^b$ is expressed as follows:

$$\tilde{x}_m^b = \sum_{p=(b-1)N_B}^{bN_B-1}\sum_{n=0}^{N_a-1} P_{m0}x_n e^{-j\frac{2\pi np}{N_a}} e^{j\frac{2\pi mp}{N}}. \tag{3.55}$$

Denoting $P_{m0}x_n$ by x_{mn}^b, $\tilde{x}_m^b$ can be written as:

$$\begin{aligned}\tilde{x}_m^b &= \sum_{p=(b-1)N_B}^{bN_B-1} DFT(x_{mn}^b)e^{j\frac{2\pi mp}{N}} \\ \tilde{x}_m^b &= IDFT(DFT(x_{mn}^b)) = x_{mn}^b.\end{aligned} \tag{3.56}$$

Therefore, by replacing $\tilde{x}_m^b$ by x_{mn}^b, we obtain:

$$s_k = \sum_{b=0}^{B}\sum_{m=0}^{N-1} x_{mn}^b f_{k-mN}^b. \tag{3.57}$$

By setting $s_k^b = \sum_{m=0}^{N-1} x_m^b f_{k-m}^b$, the UF-OFDM output signal s_k is given as:

$$s_k = \sum_{b=0}^{B} s_k^b, \tag{3.58}$$

where s_k^b is the single carrier (SC) signal at the output of the pulse shaping filter. Consequently, the precoded UF-OFDM signal is the summation of B SC signals. Although UF-OFDM signal is still a multicarrier signal, the number of the subcarriers is reduced from the IDFT size N to the number of the sub-sets B. The UF-OFDM PAPR is reduced, as it is a function of a smaller number of subcarriers.

Let us now study theoretically the way the precoding matrix reduces the PAPR of a F-OFDM signal. The precoded F-OFDM signal can be written as follows (CP is the cyclic prefix size):

$$s_k = \sum_{l=0}^{N+CP}\sum_{m=0}^{N_a-1} X_{m,l} f[k-lN] e^{j2\pi\frac{mk}{N}},$$

where

$$X_{m,l} = \sum_{n=0}^{N_a-1} P_{m0}x_{n,l}e^{-j\frac{2\pi nm}{N_a}}.$$

By setting $P_{m0}x_{n,l} = \tilde{x}_{m,l}$, we have $X_{m,l} = DFT(\tilde{x}_{m,l})$. Hence,

$$\begin{aligned}s_k &= \sum_{l=0}^{N+CP} f[k-lN]\sum_{m=0}^{N-1} DFT(\tilde{x}_{m,l})e^{j\frac{2\pi mk}{N}} \\ &= \sum_{l=0}^{N+CP} f[k-lN]IDFT(DFT(\tilde{x}_{m,l})),\end{aligned} \tag{3.59}$$

so that:

$$s_k = \sum_{l=0}^{N+CP} \tilde{x}_{m,n} f[k-lN]. \tag{3.60}$$

Therefore, s_k is the SC signal at the output of the pulse shaping filter and hence, the F-OFDM system becomes equivalent to a SC system.

In the next sections, simulation-based analysis of the signal dynamics at the input and the output of the PA are provided. First, the signal dynamics of the original modulation schemes is compared to the precoded ones in terms of two signal dynamics parameters: the PAPR and the instantaneous-to-average power ratio (IAPR). Second, the spectral shape of these signals at the PA output are presented and analyzed.

3.2.3.2 PAPR and IAPR performance

The PAPR gives an idea about the maximum input back-off (IBO) value to be taken into account to avoid the PA breakdown. Another metric to evaluate the signal dynamics is the IAPR defined by:

$$IAPR = \frac{|s_k|^2}{E[|s_k|^2]}. \tag{3.61}$$

This metric corresponds to the variation of the instantaneous measured power. Therefore, thanks to a higher granularity, it provides a better appraisal of their impact on the PA. Hence, in order to better evaluate the performance of the proposed "signal dynamics" reduction technique, we consider both metrics the IAPR and the PAPR. As after precoding the F-OFDM and the UF-OFDM are equivalent to SC signals, their PAPR and IAPR might depend on the constellation choice. For this reason, let us study the impact of the constellation choice on the PAPR and IAPR reduction. Thus the considered UF-OFDM and F-OFDM signals in this section have the parameters defined in Table 3-1.

Table 3-1: Signal parameters

DFT size: N	1024
Allocated subcarriers: N_a	480
Constellations	QPSK, 16-QAM, 64-QAM
UF-OFDM: Filter	Chebyshev
UF-OFDM: Filter length: L	72
UF-OFDM: Sidelobe attenuation	40 dB
UF-OFDM: Sub-set size: N_B	12
UF-OFDM: Sub-set number: B	40
F-OFDM: Filter	Truncated raised root cosine

In Fig. 3-29 and Fig. 3-30, the IAPR and PAPR performance using different constellations are presented. Here, the considered mother function is the rectangular filter. It should be noted that when higher order constellations are used, such as 16-QAM and 64-QAM, the PAPR reduction performance is lower than in the QPSK case. However, the performance degradation with the proposed technique is no more significant when

using 64-QAM. It shows a boundary for the PAPR and IAPR for the proposed scheme. It should be noted that with DFT-F-OFDM, we obtain as predicted better PAPR and IAPR reduction performance. Indeed, the precoding transforms the F-OFDM signal to a single carrier signal which is not the case for the UF-OFDM scheme.

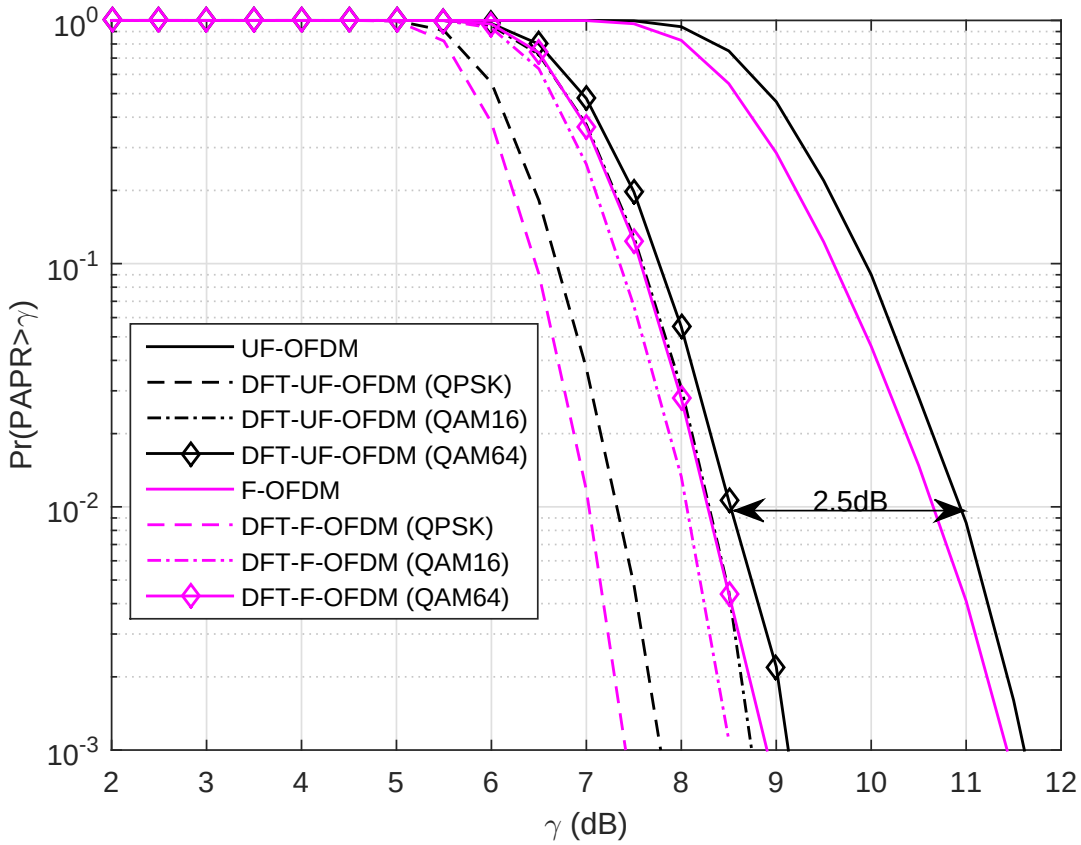

Figure 3-29: PAPR performance of the rectangular-based precoded UF-OFDM and F-OFDM schemes for different constellations.

3.2.3.3 Impact on the PA output PSD

In this part, we use the same signal characteristics for the UF-OFDM signal described in Section 3.2.3.2 and the Rapp model for the PA. In Fig. 3-31, the value of the considered IBO is 5 dB. It can be observed, from Fig. 3-31 that the tails of the spectrum of the OFDM, F-OFDM and UF-OFDM signal obtained at the output of the PA decrease slower than the tails of the spectrum of the signal at its input, which proves that the non-linearity of the PA reduces the spectral efficiency of transmitters based on these modulations. Indeed, as the generated power in the adjacent band is significant, the user of this band may be highly interfered. For this reason, a guard band has to be kept between users to avoid interferences, which may reduce the spectral efficiency.

In addition, even though the UF-OFDM and the F-OFDM PSDs are considerably lower than the OFDM signal at the PA input, they have the same level at the PA output. This is due to their similar level of PAPR. Indeed, having the same signal power level and dynamics makes the PA working at the same operating point. Therefore, the PA

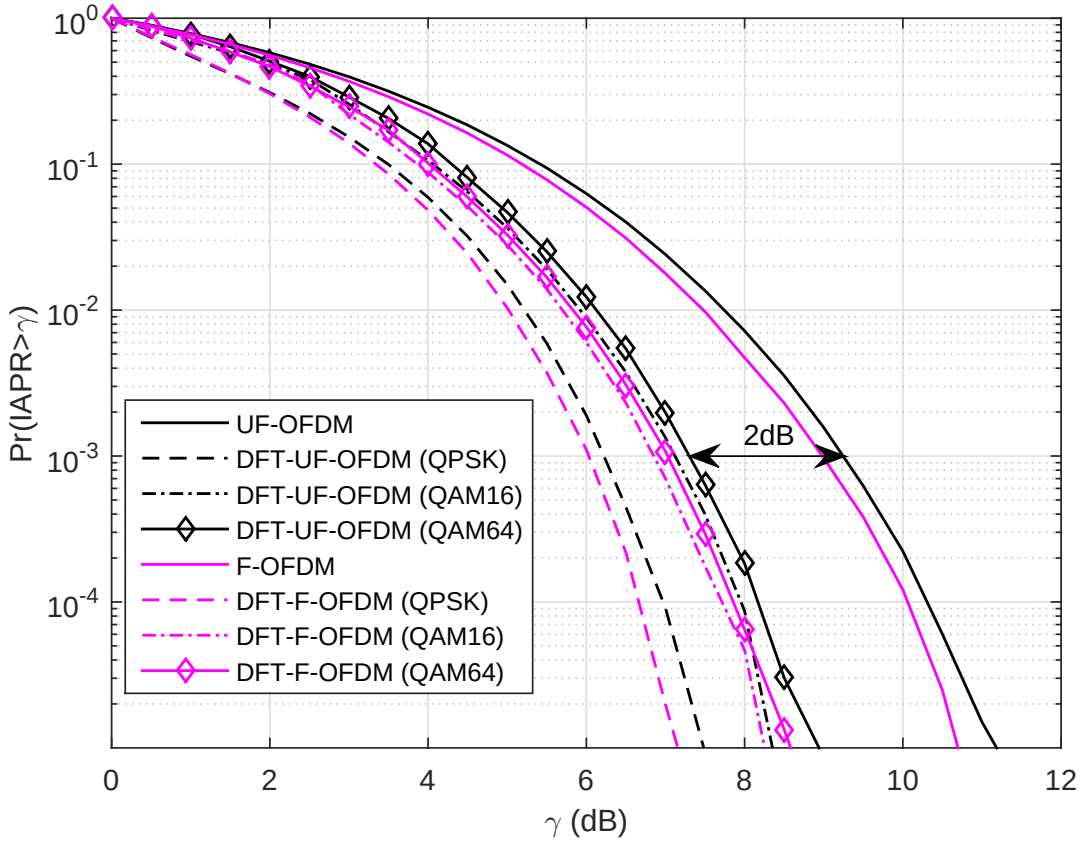

Figure 3-30: IAPR performance of the rectangular-based precoded UF-OFDM and F-OFDM schemes for different constellations.

behavior, and consequently the PA output spectral shape, are almost the same for both UF-OFDM and OFDM signals.

In Fig. 3-32, one can notice that when reducing the PAPR of the PA input signal, the PSD tails of the PA output signal are lower than the case of the original UF-OFDM signal. The different obtained PSD tails level are summarized in Table 3-2. As it can be seen from this latter, when the DFT-F-OFDM modulation scheme is used, the PSD tails are lower than the case when the DFT-UF-OFDM modulation scheme is used. This can be explained by the difference between the PAPR and IAPR levels for both schemes. Indeed, as the PAPR level of the DFT-F-OFDM is lower than the DFT-UF-OFDM one, the PA is not driven to the same operation point for the two schemes.

3.2.3.4 Complexity

While the precoding method is attractive for providing flexible PAPR reduction via adjustable precoding matrix, computational complexity will be increased rapidly with size of $L \times N$ precoding matrix, where N and L are the input and output data via precoding matrix, respectively. To overcome high complexity problem of precoding technique for PAPR reduction, this deliverable proposes a generalized precoding method to achieve low PAPR as well as low complexity. As the generalized precoding technique is applied, it achieves the same PAPR reduction with considerably lower computational complexity in comparison with that of the original precoding technique, especially for large precoded

Table 3-2: PSD-based comparison between the UF-OFDM,the F-OFDM, the DFT-UF-OFDM and the DFT-F-OFDM.

	PA output PSD tails level frequency=15.36MHz			
	UF-OFDM	F-OFDM	DFT-UF-OFDM	DFT-F-OFDM
IBO=1 dB	-17 dB	-21 dB	-20 dB	-24 dB
IBO=5 dB	-25 dB	-30 dB	-30 dB	-35 dB
IBO=9 dB	-34 dB	-39 dB	-40 dB	-47 dB

output data for further PAPR reduction. Above all, the complexity of generalized precoding method nearly approaches the complexity of the symetrical unitary matrices with $\mathcal{O}(N^2)$, and it will not increase rapidly with the complexity of non-symmetrical precoding matrix with $\mathcal{O}(LN)$.

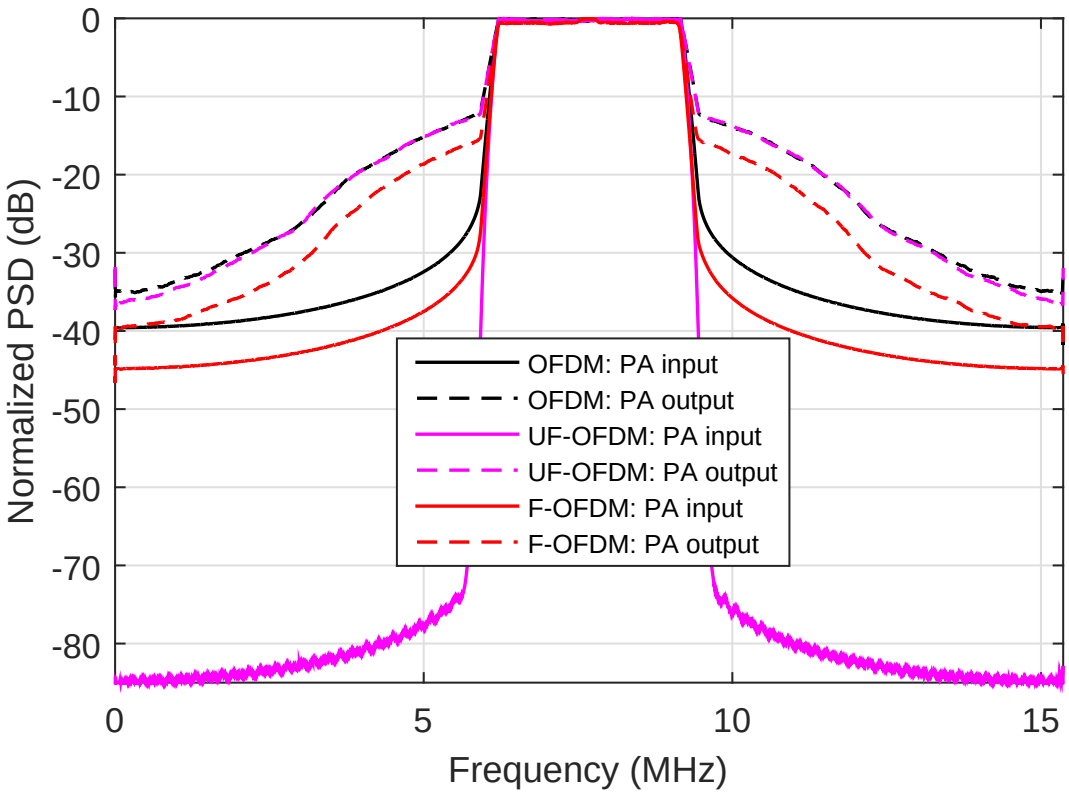

Figure 3-31: Normalized PSD-based comparison between the PA output and input signals for OFDM, F-OFDM and UF-OFDM modulations (IBO=5 dB).

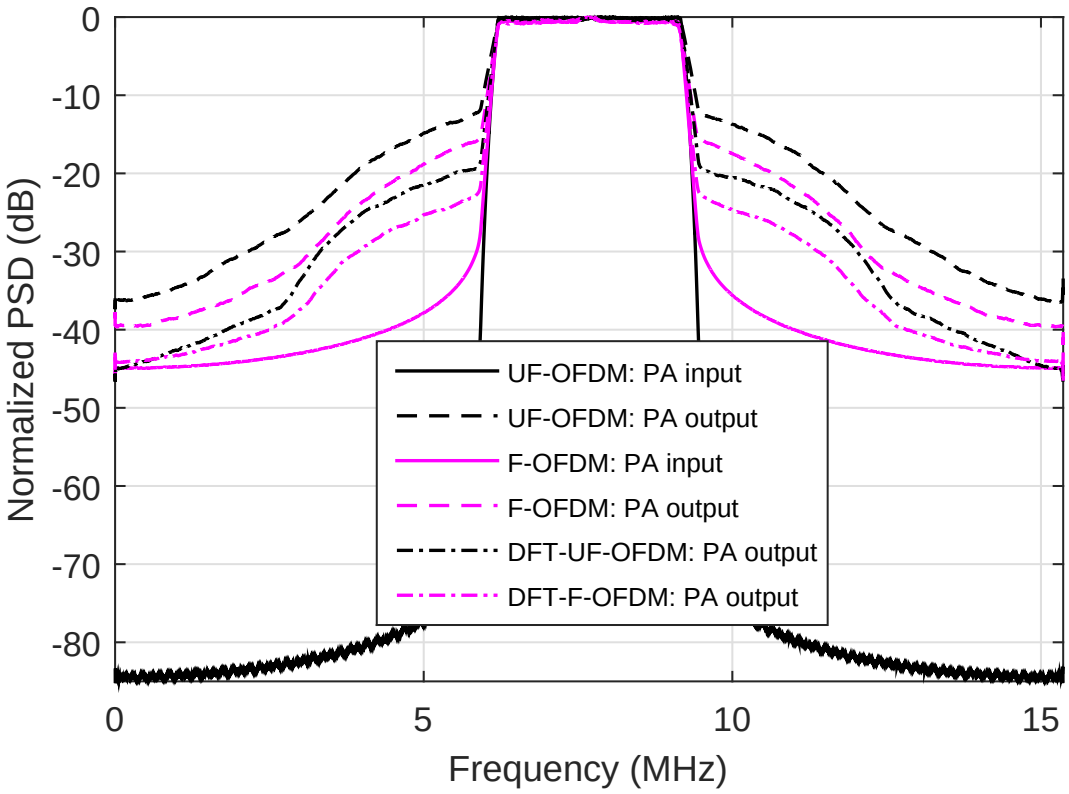

Figure 3-32: Normalized PSD-based comparison between the PA output and input signals for the UF-OFDM, the F-OFDM, the DFT-UF-OFDM and the DFT-F-OFDM (IBO=5 dB).

4. Joint methods for PAPR reduction and PA linearization techniques

4.1 State of the art

As a recall, PAPR intends to mitigate the input back-off of the power amplifier by reducing the peak power of the signal. From the other side linearization aims to make the power amplifier characteritics as linear as possible. It has often been discussed that reducing the input back-off of the power amplifier drives the signal to be amplified very closed to the saturation level where the non linearities are the more severe. So it seems natural to combine a peak power reduction method with a linearization method to enhance the power amplifier performance in terms of efficieny and linearity.

There are many ways to joint PAPR and linearization. They could be gathered in the following categories (in the following peak reduction methods will be refered as PAPR reduction method and linearization method as Digital Pre-Distortion - DPD).

- Non collaborative approach

  In this approach basic PAPR and DPD techniques are performed independantly from each others and do not exchange any information. In most of cases, PAPR is done prior to DPD. As both techniques may have opposite effets on each others, joint techniques have been investigated to enhance the overall performance. This category gathers all possible combinations of PAPR on one side and DPD on the other side.

- Collaborative approach

  In this category the principle is to make PAPR and DPD technique dependant from each others and exchange some information. For instance, PAPR technique can transmit the PAPR input and output levels to DPD algorithms ; and the DPD algorithm can transmit the compression point level to the PAPR algorithm. [HWW+10], [DJK05] are some references which update the PAPR reduction depending on the DPD algorithm outcome (in these two references, the clipping thresold of the Tone Reservation gradient algorithm is updated depending on the compression point of the power amplifier after linearisation). In [HCVG08], [GL11] and [AC16] this is the opposite : the DPD is updated depending in the PAPR of the signal after PAPR reduction (by the way of the polynomial order of the predistorter). In [RPLL06] and [Bra13] both DPD and PAPR techniques exchange information to each others. In this last reference both clipping noise and predistortion have been modeled as polynomials whose coefficients are updated according to the variations of the power amplifier characteristics. Following this idea, the authors of [LG13] proposed to model predistortion as an adding signal technique (thanks to Bussgang theorem) and to combine it with Tone Reservation which is viewed as an added signal technique. As a result, a single signal and its coefficients have to be optimized to perform both PAPR reduction and DPD. This last method is viewed as a joint PAPR and DPD approach.

Figure 4-1 summarizes the different categories to consider joint approach for PAPR and DPD.

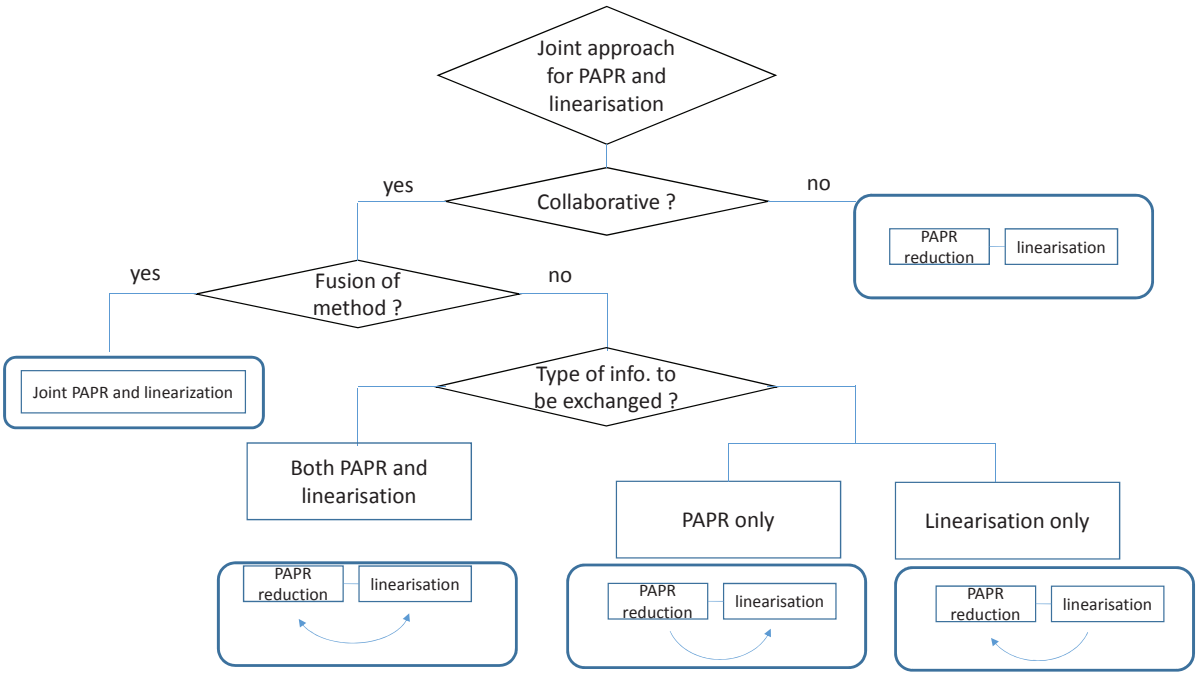

Figure 4-1: Classification of joint PAPR and DPD approaches - State of the art

4.2 Proposed method

4.2.1 Methodology

The proposed new approach is to master PAPR and DPD whose objective is first to set some performance thresolds for the overall transmission (Error Vector Magnitude -EVM, Adjacent Channel Power Ratio -ACPR, complexity, consumption, etc.). Then PAPR and DPD have to update themselves to meet the targeted criteria. In this project, the "master" block intends to set the EVM targeted value of the transmitted signal ; PAPR method is the clipping and DPD is the digital predistortion based on the identification of a polynomial which inverses the HPA characteristic. The power amplifier is based on the 3GPP HPA modeled as a polynomial function as seen in section 2.2.1. In the update process, PAPR tunes its clipping ratio and DPD the predistortion polynomial order. This is illustrated in Fig. 4-2.

4.2.2 EVM vs IBO for various clipping ratios

EVM is measured by comparing the input and output of the transmitter. EVM measurement is a way to establish the distorsions generated by the non linearities. EVM is defined as follows :

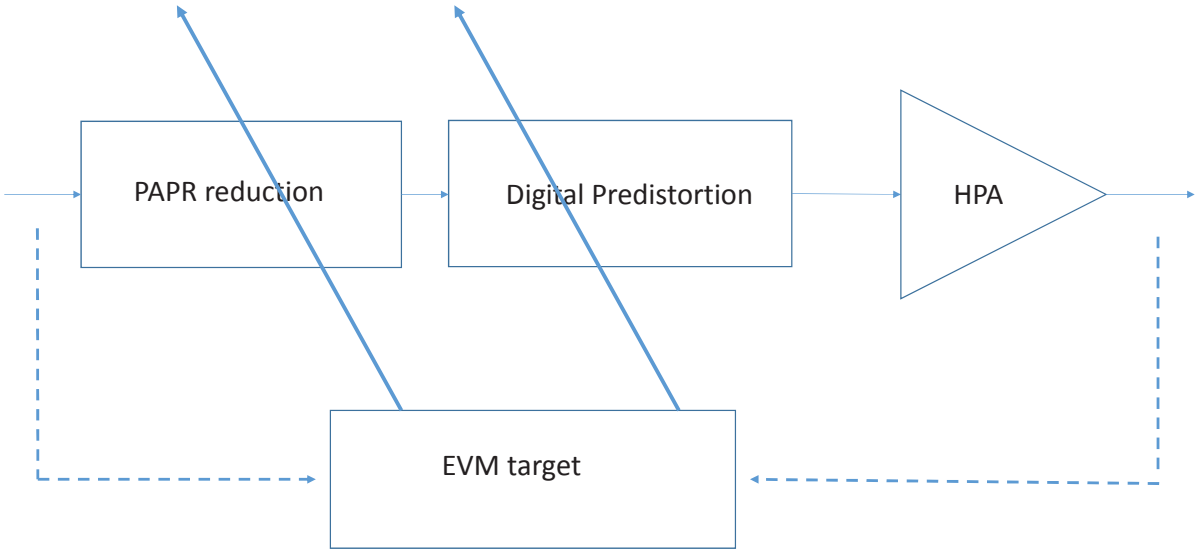

Figure 4-2: Principle of the update

$$EVM = \sqrt{\frac{E\{|x_{out}(t) - x_{in}(t)|^2\}}{E\{|x_{in}(t)|^2\}}}, \tag{4.1}$$

where $x_{in}(t)$ and $x_{out}(t)$ are the input and the output signals of the transmitter respectively. EVM is most of the time expressed in percentage. Of course the mean EVM depends on many factor : the order P of the digital predistortion polynomial $P(X)$, the order L of the power amplifier polynomial model $H(X)$, the clipping ratio CR, the IBO and the PAPR distribution of the signal to be amplified. According to these parameters, EVM has been simulated with IBO values and according to different CR values (8, 7 and 6 dB) with $L = 9$ (as set in deliverable D3.1) and P=7. The waveform used is UF-OFDM with 1024 subcarriers. The simulation results are given by Fig. 4-3.

4.2.3 EVM vs IBO for various polynomial orders

It is seen from Fig. 4-3 that there exists an IBO lower bound corresponding to the envelope of all the EVM curves. This envelope provides the optimal IBO value for a given EVM target. As a result by carrying the same simulations with different values of P (the predistortion polynomial order), we get a network of curves depending on P as sketched on Fig. 4-4. Following this it has been illustrated that for a given EVM target and a predistortion polynomial order, there is one optimal IBO value associated to the PAPR reduction gain (here the clipping ratio). By changing the IBO (while keeping the

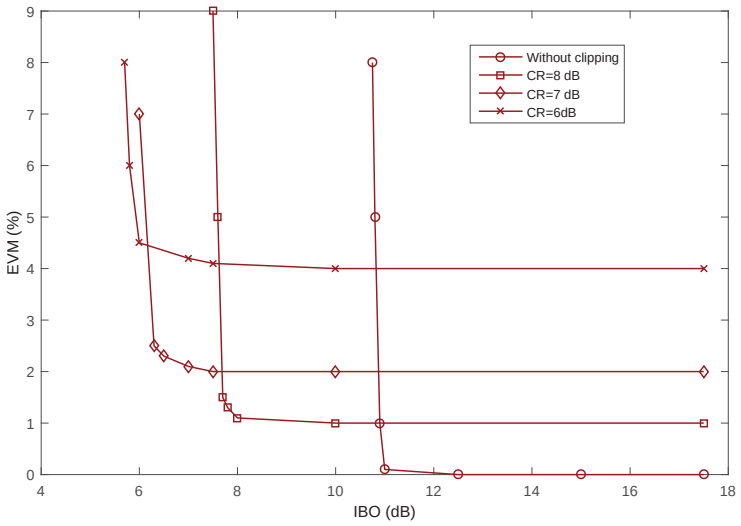

Figure 4-3: EVM as a function of IBO for P=7 - UFMC (N=1024)

same EVM value), the predistortion polynomial order can be updated accordingly.

4.2.4 Update of the state of the art of the joint classification

The proposed method gives the opportunity to update the aforementioned classification. This new approach falls in the "collaborative" category without any fusion of PAPR and DPD and without any information exchanged between these processes. Nevertheless both are mastered by a common block which tunes PAPR and DPD algorithms in parallel depending on some criteria. In this context, an new category is added to the as shown in Fig. 4-5.

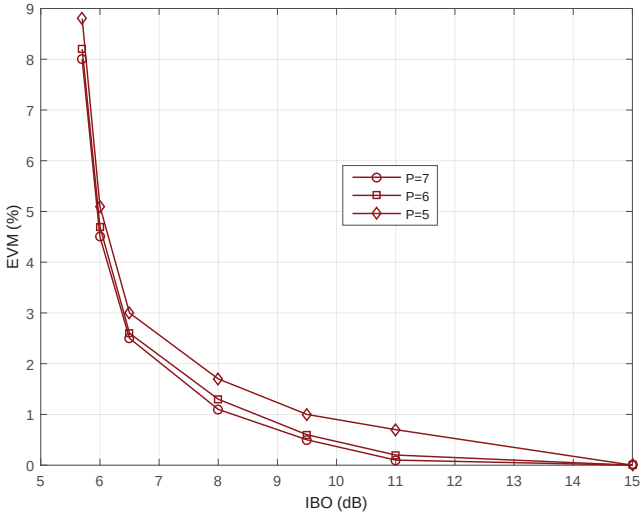

Figure 4-4: EVM as a function of IBO and P - UFMC (N=1024)

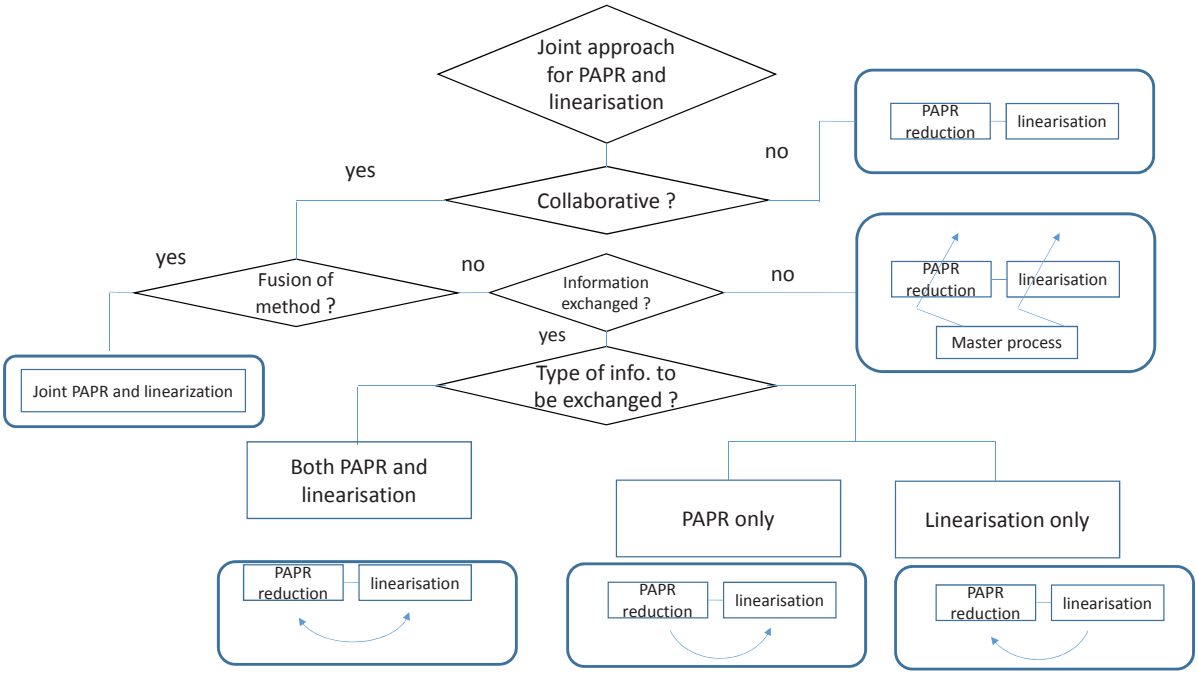

Figure 4-5: Update of the classification

5. Conclusion

This deliverable gathers the work done in the task 3.2 of WP 3. It regards the PAPR reduction of the post-OFDM waveforms UF-OFDM, F-OFDM, CP-OFDM, WOLA-OFDM and BF-OFDM. The proposed methods are based on SLM (Selected Mapping), TR (Tone Reservation) and pre-coding. This document ends with a proposal on mastering jointly PAPR reduction and DPD to target a given EVM value. This new approach allows to update a joint PAPR/DPD classifiation.

This document shows that powerfull PAPR reduction methods such as SLM, TR, precoding commonly applied to CP-OFDM can be more or les easily adapted to post-OFDM espacially when modulated symbols come to overlap. The optimal association between DPD and PAPR remains an open topic to gain both in linerity and efficiency.

Deliverable 3.3 will be covering the power budget taking into accound the hardware consumption of PAPR reduction methods and the power ampifier efficiency gain due to PAPR reduction.

6. References

[AC16] Jean-Francois Helard-Yves Louet Ali Cheaito, Matthieu Cruissiere. Energy-efficiency optimization of the high power amplifier for multicarrier systems:analytical evm derivation. *San Fransisco, USA , INFOCOM 2016*, Jul. 2016.

[AEJB94] T. A. Wilkinson A. E. Jones and S. K. Barton. Block coding scheme for reduction of peak to mean envelope power ratio of multicarrier transmission schemes. *Electronics Letters*, 25(30), Dec. 1994.

[BFH96] R. W. Bauml, R. F. H. Fischer, and J. B. Huber. Reducing the peak-to-average power ratio of multicarrier modulation by selected mapping. *IEEE Electronics Letters*, 32(22):2056–2057, Oct. 1996.

[Bra12] Mathilde Brandon. Joint optimization of linearization methods at the transmitter for multi-carrier modulations. *PhD Thesis, ETIS, Cergy Pontoise University*, Oct. 2012.

[Bra13] R.N. Braithwaite. A combined approach to digital predistortion and crest factor reduction for the linearization of an rf power amplifier. *Microwave Theory and Techniques, IEEE Transactions on*, 61(1):291–302, 2013.

[BSR15a] K. Bulusu, H. Shaiek, and D. Roviras. Potency of trellis-based slm over symbol by symbol approach in reducing ppr for fbmc-oqam signals. *IEEE ICC*, London:1–6, Jun. 2015.

[BSR15b] K. Bulusu, H. Shaiek, and D. Roviras. Reduction of papr of fbmc-oqam systems by dispersive tone reservation technique. *IEEE ISWCS*, Brussels, Aug. 2015.

[BSR16a] K. Bulusu, H. Shaiek, and D. Roviras. Pa linearization of fbmc-oqam signals with overlapped recursive error correcting predistortion. *IEEE ISWCS*, Poznan, Sep. 2016.

[BSR16b] K. Bulusu, H. Shaiek, and D. Roviras. Reducing the papr in fbmc-oqam systems with low latency trellis-based slm technique. *EURASIP Journal on Advances in Signal Processing*, Dec. 2016.

[BSRRZ17] K. Bulusu, H. Shaiek, Daniel Roviras, and M. Renfors R. Zayani. *Orthogonal Waveforms and Filter Banks for Future Communications Systems : Power Amplifier Effects and Peak-to-Average Power Ratio Mitigation*. Academic Press, Elsevier, 2017.

[Bul16] K. Bulusu. *Performance Analysis and PAPR Reduction Techniques for Filter-Bank based Multi-Carrier Systems with Non-Linear Power Amplifiers*. PhD thesis, Conservatoire National des Arts et MÃ©tiers, Paris, France, 2016.

[DJ99] J. A. Davis and J. Jedwab. Peak-to-mean power control in ofdm, golay complementary sequences, and reed-muller codes. *IEEE Transactions on Information Theory*, 7(45):2397–2417, Nov. 1999.

[DJK05] Ming Ding, Ben Jones, and Jaeweon Kim. Joint optimization of PAR reduction and digital predistortion for wireless lan applications. *Texas wireless symposium*, 2005.

[GL11] O.A. Gouba and Y. Louet. Joint study of PAPR reduction and digital predistortion. *General Assembly and Scientific Symposium, 2011 XXXth URSI*, pages 1–4, 2011.

[GP97] A. Gatherer and M. Polley. Controlling clipping probability in dmt transmission. *Asilomar Conference record*, 1:578–584, Nov. 1997.

[HCVG08] O. Hammi, S. Carichner, B. Vassilakis, and F.M. Ghannouchi. Synergetic crest factor reduction and baseband digital predistortion for adaptive 3g doherty power amplifier linearizer design. *Microwave Theory and Techniques, IEEE Transactions on*, 56(11):2602–2608, 2008.

[Hil13] Kimmo Hiltunen. Utilizing enodeb sleep mode to improve the energy-efficiency of dense lte networks. *Proc. IEEE International Symposium on Personal, Indoor and Mobile Radio Communications (PIMRC)*, Sept. 2013.

[HWW+10] Su Hu, Gang Wu, Qingsong Wen, Yue Xiao, and Shaoqian Li. Nonlinearity reduction by tone reservation with null subcarriers for WiMAX system. *Wireless Personal Communications*, 54(2):289–305, July 2010.

[JY08] T. Jiang and Y.Wu. An overview : Peak-to-average power ratio reduction techniques for ofdm signals. *IEEE Transactions on Broadcasting*, 2(54):257–268, June 2008.

[KJ03] B.S. Krongold and D.L. Jones. Par reduction in ofdm via active constellation extension. *IEEE Transactions on Broadcasting*, 3(49):258–268, Sep. 2003.

[KVH+14] Z. Kollar, L. Varga, B. Horvath, P. Bakki, and J Bito. Evaluation of clipping based iterative papr reduction techniques for fbmc systems. *Hindawi Scientific World Journal*, 841680, 2014.

[LC97] Xiaodong Li and L.J. Cimini. Effects of clipping and filtering on the performance of ofdm. *IEEE Vehicular Technology Conference*, 3:1634–1638, May 1997.

[LG13] Y. Louet and A. Gouba. Adding signal for peak to average power reduction and predistortion in an ofdm context. *IET Signal Processing*, 7(9):879–887, Jul. 2013.

[LP08] Yves Louet and Jacques Palicot. A classification of methods for efficient power amplification of signals. *Annals of Telecommunications*, 7-8(63):351–368, Jul. 2008.

[LQH13] S. Lu, D. Qu, and Y. He. Sliding window tone reservation technique for the peak-to-average power ratio reduction of fbmc-oqam signals. *IEEE Wireless Commun. Letters*, 1(4):268–271, 2013.

[MH97] S. H. Muller and J. B. Huber. Ofdm with reduced peak-to-average power ratio by optimum combination of partial transmit sequences. *IEEE Transactions on Information Theory*, 5(33):368–369, Feb. 1997.

[NMdL+14] N. V. D. Neut, B. Maharaj, F. de Lange, G. Gonzalez, F. Gregorio, and J. Cousseau. Papr reduction in fbmc using an ace-based linear programming optimization. *EURASIP Journal on Advances in Signal Processing*, 172, 2014.

[Pop91] B. M. Popovic. Synthesis of power efficient multitone signals with flat amplitude spectrum. *IEEE Transactions on Communications*, 7(39):1031–1033, Jul. 1991.

[pro16] WONG5. Wong5 project. *Deliverable 2.1: Critical and comparative study of waveforms in c-mtc context*. ANR, Tech. Rep, 2016.

[pro17a] WONG5. Wong5 project. *Deliverable 2.2: New waveforms for C-MTC context*. ANR, Tech. Rep, 2017.

[pro17b] WONG5. Wong5 project. *Deliverable 3.1: Performance of the candidate waveforms in the presence of power amplifier*. ANR, Tech. Rep, 2017.

[QLJ13] D. Qu, S. Lu, and T Jiang. Multi-block joint optimization for the peak-to-average power ratio reduction of fbmc-oqam signal. *IEEE Trans on Signal Processing*, 31(7):1605–1613, 2013.

[R4-16] R4-163314. *Realistic power amplifier model for the new radio evaluation*. 3GPP TSG-RAN WG4 Meeting No. 79, pages FS NR newRAT-Release 14, 2016.

[RPLL06] Salvatore Ragusa, Jacques Palicot, Yves Louët, and Christian Lereau. Invertible Clipping for Increasing the Power Efficiency of OFDM Amplification. *Proceedings of ICT'06*, 2006.

[SKO08] Masato Saito Satoshi Kimura, Takashi Nakamura and Minoru Okada. Par reduction for ofdm signals based on deep clipping. *3rd International Symposium on Control and Signal Processing 2008*, pages 911–916, March 2008.

[SRL06] Yves Louet Salvatore Ragusa, Jacques Palicot and Christian Lereau. Invertible clipping for increasing the power efficiency of ofdm amplification. *International Conference on Telecommunications*, 2006.

[SSJ06] A. Skrzypczak, P. Siohan, and J. P. Javaudin. Reduction of the peak-to-average power ratio for ofdm-oqam modulation. *63rd IEEE Vehicular Technology Conference*, Melbourne(4):2018–2022, 2006.

[SYLGS99] B. K. Khoo C. C. Tsimenidis S. Y. Le Goff, S. S. Al-Samahi and B. S. Sharif. Selected mapping without side information for papr reduction in ofdm. *IEEE Transactions on Wireless Communications*, 7(8):3320–3325, Jul. 1999.

[TC98] J. Tellado and J. Cioffi. Peak power reduction for multicarrier transmission. *IEEE CTMC, GLOBECOM*, Nov. 1998.

[Tel99] J. Tellado. *Peak to Average Ratio Reduction for Multi-carrier Modulation*. PhD thesis, Stanford University, Stanford, CA, USA, Sep. 1999.

[TJZ04] Guangxi Zhu Tao Jiang and Jianbin Zheng. Block coding scheme for reducing papr in ofdm systems with large number of subcarriers. *Journal of Electronics*, 6(21):482–489, 2004.

[Wun13] Gerhard Wunder. The papr problem in ofdm transmission. *IEEE Signal Processing Magazine*, pages 130–144, Nov. 2013.

Glossary and Definitions

Acronym	Meaning
AM/AM	amplitude to amplitude
AM/PM	amplitude to phase
BER	Bit Error Rate
BF-OFDM	Block Filtered OFDM
CP	Cyclic Prefix
FFT-FBMC	Fast Fourier Transform Filter Bank Multi-Carrier
f-OFDM	filtered-OFDM
HPA	High Power Amplifier
IBO	Input-Back-Off
MCM	Multi Carrier Modulation
FBMC-OQAM	FBMC with Offset Quadrature Modulation
OFDM	Orthogonal Frequency Division Multiplexing
PAPR	Peak to Average Power Ratio
PRT	Peak Reserved Tones
RRT	Ratio of Reserved Tones
DT	Data Tones
SLM	Selective Mapping
TR	Tone Reservation
UFMC (i.e. UF-OFDM)	Universal-Filtered Multi-Carrier (i.e. Universal-Filtered OFDM)
WF	WaveForm
WOLA-OFDM	Weighted Overlap and Add OFDM